




## Experimental and DFT Quantum Chemical Studies on Structural, Vibrational and Molecular Properties of Some Substituted 4-Phenylphenols

L. Ravindranath, K. Srishailam & B. Venkatram Reddy



To cite this article: L. Ravindranath, K. Srishailam & B. Venkatram Reddy (2022): Experimental and DFT Quantum Chemical Studies on Structural, Vibrational and Molecular Properties of Some Substituted 4-Phenylphenols, Polycyclic Aromatic Compounds, DOI: [10.1080/10406638.2022.2161584](https://doi.org/10.1080/10406638.2022.2161584)

To link to this article: <https://doi.org/10.1080/10406638.2022.2161584>

 View supplementary material 

 Published online: 30 Dec 2022.

 Submit your article to this journal 

 View related articles 

 View Crossmark data 



# Experimental and DFT Quantum Chemical Studies on Structural, Vibrational and Molecular Properties of Some Substituted 4-Phenylphenols

L. Ravindranath<sup>a,b</sup>, K. Srishailam<sup>c</sup>, and B. Venkatram Reddy<sup>b</sup> 

<sup>a</sup>Department of Physics, Malla Reddy Engineering College(a), Hyderabad, India; <sup>b</sup>Department of Physics, Kakatiya University, Warangal, India; <sup>c</sup>Department of Physics, SR University, Warangal, India

## ABSTRACT

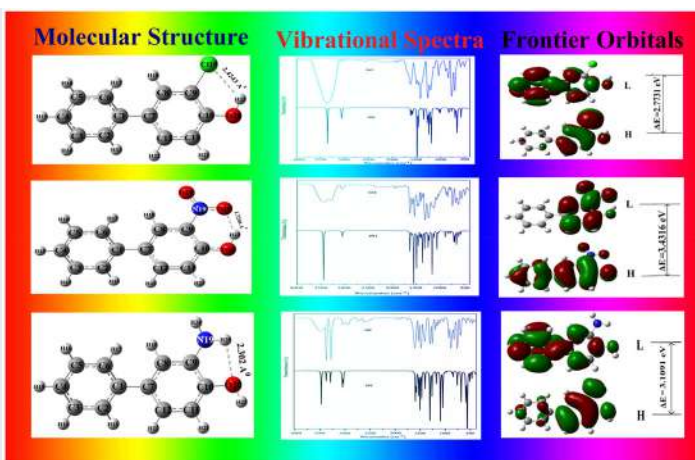
Fourier Transform infrared spectra (4000–400  $\text{cm}^{-1}$ ) and Fourier Transform Raman spectra (4000–50  $\text{cm}^{-1}$ ) were recorded for 2-chloro-4-phenylphenol (CP); 2-nitro-4-phenylphenol (NP); and 2-amino-4-phenylphenol (AP).  $^1\text{H}$  and  $^{13}\text{C}$  NMR spectra, along with UV-Vis spectra of the three samples were also measured. Quantum chemical calculations, at the level of DFT/B3LYP/6-311++G(d,p) theory were implemented to study their ground state geometry, vibrational wave numbers, infrared and Raman intensities,  $^1\text{H}$  and  $^{13}\text{C}$  NMR spectra, frontier molecular orbital parameters, NLO behavior, NBO properties, thermodynamic quantities, rotational constants and MESP behavior. TD-DFT variant was employed to simulate electronic transitions of these molecules. Observed and calculated vibrational frequencies agreed with an rms error 7.44, 8.98 and  $6.97 \text{ cm}^{-1}$ , the corresponding RMSD values being 7.09, 9.39 and  $6.59 \text{ cm}^{-1}$  for CP, NP and AP, respectively. Experimental chemical shifts concurred, with their theoretical counterparts, with RMSD value, 0.19, 0.29 and 0.56 ppm for  $^1\text{H}$  NMR; and 6.34, 6.28 and 5.39 ppm for  $^{13}\text{C}$  NMR, respectively, in CP, NP and AP. This kind of agreement was also true for absorption maxima ( $\lambda_{\text{max}}$ ) of their electronic transitions in solution form. Frontier molecular orbitals were found useful to understand origin of electronic transition maxima and chemical reactivity of the three molecules which was supported by NBO analyses. The computations showed that the three molecules were potentially good for developing NLO materials. MESP investigations showed that the most reactive sites are at oxygen atoms in the three molecules. Moreover, we also made an attempt to understand the effect of deactivating (Cl,  $\text{NO}_2$ ) and activating ( $\text{NH}_2$ ) groups on certain properties of the three molecules. Presence of intra-molecular hydrogen bond was predicted in CP, NP and AP.

## ARTICLE HISTORY

Received 27 September 2022  
Accepted 16 December 2022

## KEYWORDS

4-Phenylphenol; DFT; vibrational spectra; NMR spectra; NBO analysis



### HIGHLIGHTS

- Structure parameters for CP, NP and AP agree well with their experimental counterparts.
- Computed and measured frequencies, chemical shifts and electronic transitions agree acceptably.
- Effect of activating and deactivating groups is studied.
- CP, NP and AP are potential NLO materials.
- Intra-molecular charge transfer (ICT) is demonstrated using NBO analysis.

## 1. Introduction

We know that 4-phenylphenol or 4-hydroxyphenyl, a derivative of the representative molecule biphenyl (BP) can be considered as a basic unit for its chloro-, nitro-, and amino derivatives. In this article we considered three such substituted hydroxybiphenyls. These are 2-chloro-4-phenylphenol (CP); 2-nitro-4-phenylphenol (NP); and 2-amino-4-phenylphenol (AP). Nitrophenylphenols were known for their herbicidal activity, which showed significant increase with progressive substitution of nitro groups on non-phenolic ring.<sup>1</sup> Extension of these investigations to chlorophenylphenols revealed that the herbicidal characteristics were influenced remarkably with increasing number of chlorine atoms on the phenylphenol ring.<sup>2</sup> Further, chloro derivatives of 4-phenylphenol along with their basic value were found highly effective fungistatic agents against *Aspergillus niger* and *Piricularia oryzae*, arising from their reactivity, steric repulsion, permeability and metabolic simulation.<sup>3</sup> Miticidal activity of phenylphenols was correlated with their molecular structure,<sup>4</sup> which was found sensitive to the position of substitution and number of substituents such as chlorine atoms, nitro groups and amino moieties.<sup>5-7</sup> Several antimicrobial agents found in biosolids were identified as derivatives of chlorinated phenylphenols.<sup>8</sup> X-ray structure of 4-hydroxybiphenyl is also available.<sup>9</sup> From existing literature we find that the earlier studies were confined mainly to exploring biological activity, comprising of antimicrobial,<sup>10,11</sup> antiproliferative,<sup>12</sup> estrogenic,<sup>13</sup> antioxidant,<sup>14</sup> metabolic<sup>15,16</sup> and antimalarial<sup>17</sup> properties, of CP, NP, AP and their derivatives. Molecular structure, either experimental or theoretical, is not reported in literature for CP, NP and AP. This is also the case with normal coordinate analysis and other important molecular parameters for the three molecules. Against this backdrop we undertook the work reported in this article with the objectives: (i) to investigate molecular structure of CP, NP and AP in gas phase by employing DFT/B3LYP/6-311++G(d,p) formalism, (ii) to perform normal coordinate analysis making use of measured infrared and Raman spectra, evaluating general valence force field in the process, in order to assign all

observed vibrational fundamentals unambiguously, (iii) to record  $^1\text{H}$  and  $^{13}\text{C}$  NMR spectra and compare them with corresponding theoretical counterparts, (iv) to use frontier molecular orbitals to help assign observed electronic spectra and to gain some insight into chemical reactivity, (v) to evaluate nonlinear optical (NLO) parameters, in order to examine utility of the compounds for nonlinear applications, (vi) to make natural bond orbital analyses, so as to understand origin of the stabilizing energy, (vii) to compute molecular electrostatic surface potentials, in order to identify reactive sites, and (viii) to estimate thermodynamic quantities for future use. Further, we wish to examine the effect of presence of activating or electron donating ( $\text{NH}_2$ ) and deactivating or electron withdrawing ( $\text{NO}_2$  and  $\text{Cl}$ ) groups on the phenolic ring of 4-phenylphenol on certain properties of CP, NP and AP. It is to be stated that the effect of activating and deactivating moieties on molecular properties was reported earlier by Castillo et al.,<sup>18</sup> for a different molecule. In this way, this article constitutes a significant addition to the existing knowledge regarding CP, NP and AP.

## 2. Experimental methods

Samples of CP and AP were purchased from TCI chemical company, Japan, whereas NP was obtained from Sigma Aldrich Chemical Company, USA as high purity chemicals. Hence, they were used as received, without further purification, for spectral measurements. The samples were solids at room temperature. Therefore, their FTIR spectra were measured by diluting the samples in KBr pellet, using JASCO FTIR-4200 Model spectrometer in the  $4000\text{--}400\text{ cm}^{-1}$  region with resolution  $\pm 0.5\text{ cm}^{-1}$ . The FT Raman spectra of the three compounds were recorded employing BRUKER RFS27 model interferometer accessory in the  $4000\text{--}50\text{ cm}^{-1}$  strokes region with  $\pm 2\text{ cm}^{-1}$  resolution using with the exciting radiation at 1064 nm provided by Nd-YAG laser operating at 200 mW power.  $^1\text{H}$  and  $^{13}\text{C}$  NMR spectra were obtained with the help of Bruker's AV NEO Spectrometer at 400 MHz in solution of deuterated chloroform ( $\text{CDCl}_3$ ) for CP and NP; and dimethylsulfoxide- $d_6$  ( $\text{DMSO-}d_6$ ) was the solvent for AP. The chemical shifts were obtained in ppm units using TMS as internal standard. The UV-Visible spectra of the three samples were measured with Jasco UV-670 spectrophotometer in the range 500–190 nm using quartz cell of 1 cm path length in a solution of  $\text{CDCl}_3$  for CP and NP, whereas the same measurement for AP was made in solution of  $\text{DMSO-}d_6$ . Purity of all chemicals and reagents was of spectro grade. All spectral measurements were made at room temperature.

## 3. Computational considerations

Quantum chemical calculations were carried out by make use of density functional theory (DFT) method. Becke's non-local gradient approach with three parameter hybrid density exchange functional (B3)<sup>19</sup> in association with Lee, Young and Parr gradient corrected correlation functional (LYP)<sup>20</sup> in combination with triple zeta split-valence basis set, 6-311++G(d,p) was employed for computations using Gaussian 09 software.<sup>21</sup> The geometry optimization is generally done by initiating the starting structure of a given molecule. But both experimental and theoretical structures are not available for CP, NP and AP. In such cases, it is customary to use Gauss view<sup>22</sup> to generate an initial structure of the given molecule. Hence, the initial structure parameters, viz, bond lengths, bond angles and dihedral angles for CP, NP and AP were borrowed from Gauss view<sup>22</sup> library, except the dihedral angles associated with C–C inter-ring bond, phenolic C–O bond in the three molecules, and C–N carbon-nitrogen bond in NP and AP, as the database available with gauss view<sup>22</sup> is not sufficient to provide reliable values for these dihedrals. For instance, according to gauss view,<sup>22</sup> dihedral angle around C–C inter-ring bond is  $0^\circ$  for the three molecules, whereas its experimental value for the representative molecule, biphenyl is  $44.4^\circ$ , as determined from electron diffraction experiments.<sup>23</sup> Hence, the torsion angle around C–C inter-ring bond was taken from biphenyl<sup>23</sup> for the three molecules, whereas that associated with phenolic

C–O bond was transferred from experimental value reported for 4-methoxy-3-nitrobiphenyl.<sup>24</sup> Similarly, the torsion angle for C–N bond in AP was borrowed from experimental value available for 3, 3', 4, 4'-tetraaminobiphenyl,<sup>25</sup> while that corresponding to the C–N bond was taken from 4-methoxy-3-nitrobiphenyl.<sup>24</sup> The initial structures obtained in this way were subjected to rigorous geometry optimization by relaxing all structure parameters simultaneously; allowing the process to get terminated on achieving default convergence criterion as defined in Gaussian 09 program suit.<sup>21</sup> This procedure resulted in non-planar structure of C<sub>1</sub> symmetry for CP, NP and AP. Absence of negative frequencies stands as testimony for the reliability of above result for the optimized structures. It is to be noted that the calculations were performed on a single molecule, each of CP, NP and AP, in the gas phase.

Using C<sub>1</sub> structure as equilibrium geometry for CP, NP and AP, the harmonic vibrational frequencies, cartesian force constants and dipole moment along with its derivatives were evaluated. Further computations were carried out using the equilibrium geometry and resultant final force constants. Employing MOLVIB 7.0 Program,<sup>26,27</sup> the force constants were transformed into a non-redundant set of 63, 69 and 69 natural internal coordinates for CP, NP and AP, respectively. These were constructed from redundant internal coordinates following the procedure suggested by Fogarasi et al.<sup>28</sup> Scaling of force constants was made using least-square refinement procedure suggested by Pulay and Fogarasi<sup>29</sup> and Arenas et al.<sup>30</sup> so as to achieve the best possible fit between observed and calculated wave numbers for these molecules. In order to characterize the normal modes of vibration, the fundamental frequencies, corresponding eigenvectors, potential energy distribution (PED), relative IR absorption intensities<sup>31</sup> and relative Raman scattering intensities<sup>32,33</sup> were computed. To compare experimental IR and Raman spectra with their theoretical counterparts for CP, NP and AP, pure Lorentzian band shape with full width at half maximum (FWHM) of 10 cm<sup>-1</sup> was used in the simulation process.

NMR spectra (<sup>1</sup>H and <sup>13</sup>C Chemical shifts) were computed employing gauge-independent or gauge-including atomic orbital (GIAO) approach<sup>34</sup> with DFT/B3LYP/6-311++G(d,p) method. Resulting simulated NMR spectra of the three molecules were compared with corresponding observed spectra by making linear regression plots. To simulate electronic absorption spectra of CP, NP and AP, time-dependent density functional theory (TD-DFT) was used employing B3LYP/6-311++G(d,p) formalism. Calculated values of absorption maxima ( $\lambda_{\text{max}}$ ) were identified with their corresponding observed values in UV–Vis spectra. Solvent effects, in both NMR and UV–Vis spectra were taken care of by the Polarizable Continuum Model (PCM) using the integral equation formalism (IEF-PCM) variant<sup>35</sup> integrated into Gaussian 09 software package.

Using frontier molecular orbital energies, comprising of the highest occupied molecular orbital (HOMO) and the lowest unoccupied molecular orbital (LUMO), the values for molecular electronic properties of CP, NP and AP such as ionization potential (*I*), electron affinity (*A*), global hardness ( $\eta$ ), chemical potential ( $\mu$ ), and global electrophilicity power ( $\omega$ ) were determined using well-known expressions.<sup>36–38</sup>

NLO behavior of the molecules CP, NP and AP was studied by computing the total molecular dipole moment ( $\mu_t$ ) and its components, total molecular polarizability ( $\alpha_t$ ) and its components, anisotropy of polarizability ( $\Delta\alpha$ ), and first order static hyperpolarizability ( $\beta_1$ ) using density functional theory following Buckingham's definitions<sup>39</sup> and DFT/B3LYP/6-311++G(d,p) level of theory. Similarly, thermodynamic parameters and rotational constants were determined and the molecular electrostatic surface potential (MESP) was investigated by mapping of molecular electrostatic potential.

Natural bond orbital (NBO) analysis was performed using NBO 3.1 program<sup>40</sup> as implemented in the Gaussian 09 package with the 6-311++G(d,p) basis set, in order to understand various second order interactions between the filled orbitals of one subsystem and vacant orbitals of another subsystem using second-order perturbation theory as revealed by Fock matrix analysis. The stabilization energy associated with the hyper conjugation is evaluated using the equation given by Glendening et al.<sup>40</sup>

## 4. Results and discussion

### 4.1. Molecular geometry in the ground state and intra-molecular hydrogen bond

Ground state molecular geometry of CP, NP and AP is dictated by two opposing effects. These are:

1. The  $\pi$ -electron delocalization between the two phenyl rings favors a co-planar structure. This is further strengthened by participation of lone pair electrons from oxygen atom of activating OH moiety in the three molecules. In addition, lone pairs from deactivating chlorine atom in CP; corresponding pairs from two oxygen atoms and one nitrogen atom from deactivating nitro group in NP, along with similar electrons associated with nitrogen atom in activating amino moiety in AP take part in stabilizing the planar structure, and
2. The steric repulsion of
  - two pairs of ortho hydrogens, neighboring the inter-ring C–C bond;
  - ortho hydrogen and hydroxyl group,
  - ortho hydrogen on X, where X is Cl, NO<sub>2</sub> and NH<sub>2</sub> in CP, NP and AP, respectively, and
  - ortho hydroxyl moiety and hence X,

favors a non-planar structure, in order to minimize steric effects. The most stable rotamer of either CP or NP or AP is a result of equilibrium between these two opposing effects. Relative contributions of the above effects determine the dihedral angle around inter-ring C–C bond / phenolic C–O bond / nitro C–N bond / amino C–N bond. This sensitive balance is greatly influenced by two factors:

- i. the amount of correlation energy that the theoretical formalism can accommodate, and
- ii. The size of basis set used for the computations.<sup>41–43</sup>

Initial values of dihedral angles associated with inter-ring C–C bond, phenolic C–O bond, nitro C–N bond and amino C–N bond were transferred from related molecules<sup>23–25</sup> as already stated. These were (44.4° and 178.07°) for CP (note that there is no C–N bond in CP); (44.4°, 178.07° and 27.5°) for NP; and (44.4°, 178.07° and 26°) for AP. They were refined to (40.56° and 0.093°) for CP; (39.720°, 0.520° and 0.951°) for NP and (40.29°, 176.71° and 26.74°) for AP, on optimization.

The torsional angles of C–C inter-ring bond at 40.56°, 39.72° and 40.29° for CP, NP and AP, respectively, are close to their initial value borrowed from BP at 44.4° determined from electron diffraction experiments.<sup>23</sup> They also agree well with that of BP at 42° obtained from DFT/B3LYP/6-311++G(d,p) calculations,<sup>44</sup> which is the same formalism used in the present article. This is expected as the steric repulsion arises from the same set of two pairs of ortho hydrogens neighboring the C–C inter-ring bond in the four molecules BP, CP, NP and AP. Further, occurrence of twist angles of C–C inter-ring bond at lower values in comparison with that of BP should be attributed to the presence of activating OH and NH<sub>2</sub> groups and deactivating Cl and NO<sub>2</sub> species in the molecules under consideration. The difference between twist angles of C–C inter-ring bond for CP and NP is the difference between 40.56° and 39.72°, which is 0.84°. Justification of this difference is not attempted, as it is significantly less than the RMSD value for dihedral angles reported in this article around 2° (see Table 1). The same explanation applies equally well for similar difference between same quantities for CP and AP; and NP and AP. Optimized values of torsion angles around phenolic C–O bond are near 0.093°, 0.520° and 176.71° for CP, NP and AP, respectively. We assumed *trans* position for hydrogen atom of hydroxyl moiety with respect to amino group nitrogen atom in AP, initially (see Figure 1). If we were to start with *cis* position for the hydrogen atom, the separation between this atom and the nearest amino hydrogen atom

**Table 1.** Experimental and DFT/B3LYP/6-311 ++ G(d,p) optimized geometric parameters of CP, NP and AP.

Geometric parameter	Calculated value			Experimental value	
	CP	NP	AP	Ref. <sup>9</sup>	Ref. <sup>24</sup>
Bond lengths (in Å)					
C1–C2	1.403	1.403	1.403	1.389	1.381
C2–C3	1.392	1.392	1.392	1.392	1.376
C3–C4	1.394	1.394	1.394	1.374	1.358
C4–C5	1.394	1.394	1.394	1.359	1.363
C5–C6	1.392	1.392	1.392	1.387	1.377
C6–C1	1.403	1.402	1.403	1.389	1.383
C1–C7	1.485	1.484	1.485	1.488	1.473
C7–C8	1.400	1.388	1.402	1.399	1.387
C8–C9	1.388	1.400	1.396	1.386	1.370
C9–C10	1.398	1.414	1.407	1.369	1.398
C10–C11	1.396	1.403	1.387	1.359	1.385
C11–C12	1.387	1.380	1.394	1.386	1.370
C12–C7	1.404	1.413	1.399	1.383	1.384
C2–H13	1.084	1.084	1.084	*	0.930
C3–H14	1.084	1.084	1.085	*	0.930
C4–H15	1.084	1.084	1.084	*	0.930
C5–H16	1.084	1.084	1.085	*	0.930
C6–H17	1.084	1.084	1.084	*	0.930
C8–H18	1.082	1.081	1.085	*	0.930
C9–C19	1.766	–	–	1.401 <sup>a</sup>	–
C9–N19	–	1.453	–	*	1.459
C9–N19	–	–	1.394	*	1.40 <sup>p</sup>
C10–O20	1.357	1.337	1.378	1.385	1.336
C11–H21	1.083	1.083	1.086	*	0.930
C12–H22	1.083	1.084	1.083	*	0.930
O20–H23	0.967	0.982	0.962	0.968 <sup>a</sup>	–
N19–O24	–	1.219	–	*	1.209
N19–O25	–	1.248	–	*	1.215
N19–H24	–	–	1.009	0.9 <sup>b</sup>	–
N19–H25	–	–	1.009	0.9 <sup>b</sup>	–
RMSD	0.094	0.088	0.094		
Bond angle (in °)					
C1–C2–C3	120.91	120.84	121.03	121.4	121.3
C2–C3–C4	120.28	120.24	120.30	120.7	120.8
C3–C4–C5	119.44	119.51	119.36	118.7	119.1
C4–C5–C6	120.27	120.26	120.30	120.9	120.7
C5–C6–C1	120.92	120.82	121.03	121.8	121.1
C6–C1–C2	118.17	118.32	117.99	116.4	117.07
C7–C8–C9	120.43	121.03	122.09	121.3	120.92
C8–C9–C10	121.69	121.37	120.50	120.4	121.36
C9–C10–C11	117.96	117.17	118.14	119.7	116.20
C10–C11–C12	120.58	120.99	120.57	119.9	121.33
C11–C12–C7	121.53	122.01	120.25	121.8	122.37
C12–C7–C8	117.80	117.42	118.43	116.8	116.83
C2–C1–C7	120.82	120.77	120.94	*	120.93
C6–C1–C7	121.00	120.90	121.07	*	121.99
C8–C7–C1	120.78	121.36	120.55	*	121.15
C12–C7–C1	121.41	121.22	121.01	*	122.02
C1–C2–H13	119.53	119.70	119.37	*	119.4
C3–C2–H13	119.54	119.43	119.58	*	119.4
C2–C3–H14	119.65	119.67	119.65	*	119.6
C4–C3–H14	120.06	120.09	120.04	*	119.6
C3–C4–H15	120.28	120.24	120.32	*	120.5
C5–C4–H15	120.28	120.24	120.31	*	120.5
C4–C5–H16	120.07	120.09	120.04	*	119.7
C6–C5–H16	119.66	119.65	119.67	*	119.7
C5–C6–H17	119.52	119.53	119.54	*	119.4
C1–C6–H17	119.54	119.63	119.40	*	119.4
C7–C8–H18	120.50	121.17	119.47	*	119.5
C9–C8–H18	119.05	117.79	118.42	*	119.5

(continued)



Table 1. Continued.

Geometric parameter	Calculated value			Experimental value	
	CP	NP	AP	Ref. <sup>9</sup>	Ref. <sup>24</sup>
C8–C9–C19	119.97	–	–	119.50 <sup>a</sup>	–
C10–C9–C19	118.34	–	–	119.10 <sup>a</sup>	–
C8–C9–N19	–	117.89	122.38	–	116.53
C10–C9–N19	–	120.73	119.48	–	121.11
C9–C10–O20	123.45	124.83	115.94	*	124.48
C11–C10–O20	118.58	117.99	123.56	*	119.30
C10–C11–H21	118.21	117.65	119.45	*	119.3
C12–C11–H21	121.20	121.36	119.97	*	119.3
C11–C12–H22	118.97	118.79	119.51	*	118.8
C7–C12–H22	119.48	119.18	120.20	*	118.8
C10–O20–H23	109.27	107.30	109.82	*	–
C9–N19–O24	–	119.37	–	*	119.17
C9–N19–O25	–	117.88	–	*	117.51
C9–N19–H24	–	–	115.76	109.9 <sup>b</sup>	–
C9–N19–H25	–	–	114.94	104.3 <sup>b</sup>	–
RMSD	0.722	0.786	0.823		
Dihedral angle (in °)					
C1 – C2 – C3 – C4	–0.147	–0.024	–0.157	*	–0.3
C2 – C3 – C4 – C5	0.075	0.019	0.095	*	1.0
C3 – C4 – C5 – C6	0.065	0.038	0.057	*	1.6
C4 – C5 – C6 – C1	–0.135	–0.092	–0.150	*	–1.0
C5 – C6 – C1 – C2	0.063	0.086	0.089	*	0.3
C6 – C1 – C2 – C3	0.077	0.029	0.065	*	0.9
C7 – C8 – C9 – C10	–0.188	–0.437	–0.016	*	–0.7
C8 – C9 – C10 – C11	0.177	0.421	0.128	*	0.7
C9 – C10 – C11 – C12	–0.101	–0.190	–0.188	*	–0.3
C10 – C11 – C12 – C7	0.039	0.033	0.099	*	0.0
C11 – C12 – C7 – C8	–0.045	–0.033	–0.044	*	0.0
C12 – C7 – C8 – C9	0.117	0.198	0.102	*	0.4
C12 – C7 – C1 – C6	–139.44	–140.33	–139.46	*	–144.19
C8 – C7 – C1 – C6	40.56	39.72	40.29	44.4 <sup>b</sup>	36.2
C12 – C7 – C1 – C2	40.53	39.67	40.61	*	36.6
C8 – C7 – C1 – C2	–139.46	–140.28	–139.78	*	–143.06
C6 – C1 – C2 – H13	–178.42	–178.43	–178.48	*	*
C4 – C3 – C2 – H13	178.35	178.38	178.39	*	*
C1 – C2 – C3 – H14	–179.51	–179.42	–179.53	*	*
C5 – C4 – C3 – H14	179.43	179.41	179.47	*	*
C2 – C3 – C4 – H15	179.95	179.98	179.92	*	*
C6 – C5 – C4 – H15	–179.91	–179.92	–179.93	*	*
C3 – C4 – C5 – H16	179.44	179.47	179.40	*	*
C1 – C6 – C5 – H16	–179.51	–179.53	–179.49	*	*
C4 – C5 – C6 – H17	178.33	178.46	178.30	*	*
C2 – C1 – C6 – H17	–178.40	–178.46	–178.36	*	*
C12 – C7 – C8 – H18	–178.40	–178.58	–178.69	*	*
C10 – C9 – C8 – H18	178.35	178.39	178.62	*	*
C7 – C8 – C9 – C19	–179.50	–	–	*	*
C11 – C10 – C9 – C19	179.50	–	–	*	*
C7 – C8 – C9 – N19	–	–179.75	–177.92	*	–179.67
C11 – C10 – C9 – N19	–	179.71	177.84	*	179.73
C8 – C9 – C10 – O20	–179.90	–179.81	–179.41	*	*
C12 – C11 – C10 – O20	179.98	179.97	179.31	*	*
C9 – C10 – C11 – H21	179.26	179.18	179.36	*	*
C7 – C12 – C11 – H21	–179.31	–179.38	–179.45	*	*
C10 – C11 – C12 – H22	178.54	178.69	178.37	*	*
C8 – C7 – C12 – H22	–178.54	–178.69	178.21	*	*
C8 – C9 – N19 – O24	–	0.951	–	*	27.5
C10 – C9 – N19 – O24	–	–179.73	–	*	–152.12
C8 – C9 – N19 – O25	–	–179.20	–	*	–149.80
C10 – C9 – N19 – O25	–	0.115	–	*	30.6
C8 – C9 – N19 – H24	–	–	26.74	26.9 <sup>b</sup>	*
C10 – C9 – N19 – H24	–	–	155.37		*

(continued)



Table 1. Continued.

Geometric parameter	Calculated value			Experimental value	
	CP	NP	AP	Ref. <sup>9</sup>	Ref. <sup>24</sup>
C8 – C9 – N19 – H25	–	–	161.85	*	*
C10 – C9 – N19 – H25			20.27	*	*
C9 – C10 – O20 – H23 <sup>c</sup>	0.093	0.520	176.71	*	178.07
C11 – C10 – O20 – H23 <sup>d</sup>	179.99	179.71	2.81	*	*
RMSD	2.108	1.815	2.086		

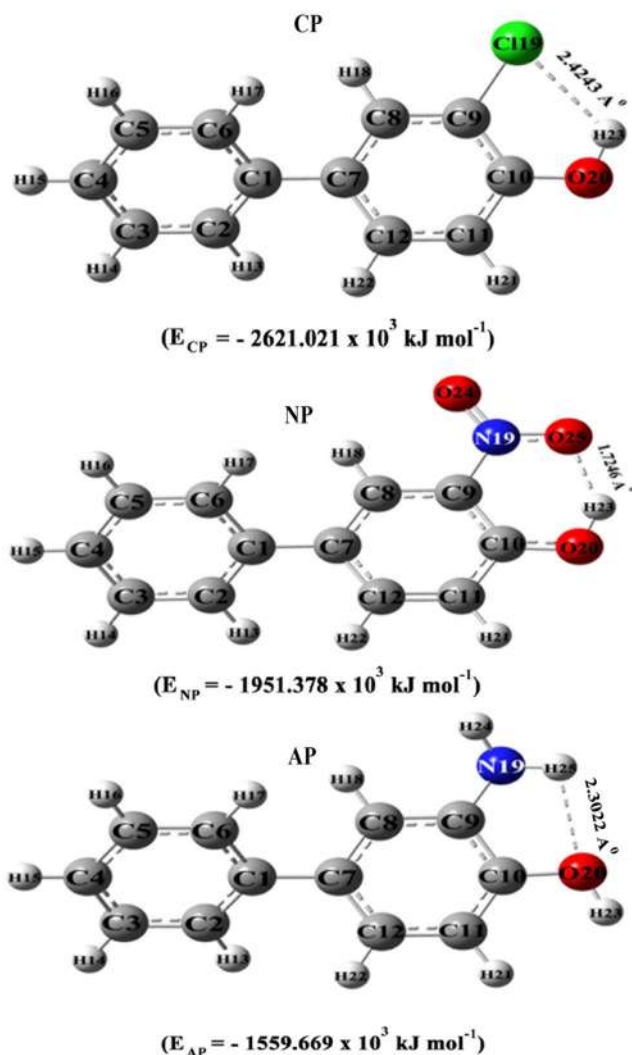
  

Bifurcated intramolecular hydrogen bond geometry (bond length in Å; bond and dihedral angles in degrees) for CP, NP, and AP						
Molecule	DH...A	D–H	H...A	D...A	∠D–H...A	∠D–H...A–X <sup>e</sup>
CP	O20–H23...C19	0.967	2.424	3.014	119.04	0.50
NP	O20–H23...O25	0.982	1.725	2.575	142.71	0.53
AP	N19–H25...O20	1.010	2.302	2.695	101.64	165.82

–: Not relevant; \*: Not available. a: from reference 44. b: Experimental value from reference 25. c: *cis* angle in (CP and NP) and *trans* angle in AP. d: *trans* angle in (CP and NP) and *cis* angle in CP. e: X = C9 in CP, N19 in NP, and H23 in AP.

being short at 1.5 Å could have pushed hydroxyl hydrogen atom into the *trans* position due to strong steric repulsion between the hydrogen atoms under consideration. In fact geometry optimization confirmed our assumption. This explains the agreement of initial value at 178.07° and final value near 176.71° for AP. However, the corresponding values, 0.093° and 0.520° for CP and NP, respectively are not comparable to their initial value at 178.07°, which is transferred from 4-methoxy-3-nitrophenyl.<sup>24</sup> During the optimization it was assumed that the hydrogen atom of hydroxyl moiety is in *trans* position with respect to the nitrogen atom of the nitro group in NP, and with respect to the chlorine atom in CP as in AP. In this position the separation between the hydrogen atom of hydroxyl group and the nearest hydrogen atom of the phenyl ring is 2.05 Å and 2.14 Å in NP and CP, respectively. Steric repulsion, being strong enough to negate attraction due to formation of intra-molecular hydrogen bond between these hydrogen pairs pushes the hydrogen atom of the hydroxyl moiety into the *cis* position in both the molecules NP and CP (see Figure 1). It is to be noted, that the *trans* dihedral angle and the *cis* dihedral angle for a given bond in a molecule are mutually supplementary. Hence, initial value for dihedral angle for NP and CP can be obtained by subtracting *trans* dihedral angle 178.07°, taken from reference number 24, from 180°. This comes out to be 1.93°, which compares reasonably well with final values at 0.520° and 0.093° for NP and CP, respectively. Thus, the seemingly absurd values can be explained. The optimized value of torsion angle around nitro C–N bond in NP is at 0.951°, whereas its initial value borrowed from 4-methoxy-3-nitrophenyl<sup>24</sup> is 27.5°. Steric repulsion is the cause for this significant difference between the initial and optimized value. The steric repulsion exerted by the bulky methoxy group on the adjacent nitro moiety in 4-methoxy-3-nitrophenyl is considerably higher than that exerted by relatively small hydroxyl molecular fragment on the nitro group in NP, making the dihedral angle in the former molecule is significantly greater than the corresponding angle in the latter molecule. Initial value of amino C–N bond at 26° taken from 3,3',4,4'-tetra amino biphenyl<sup>25</sup> in AP agrees nicely with its optimized value near 26.74°.

Optimized molecular geometries generated as a result of solving self-consistent field equations for CP, NP and AP are shown in Figure 1, along with numbering of atoms. Corresponding structure data consisting of bond lengths, bond angles and dihedral angles for the molecules are presented in Table 1. This table also contains information about intra-molecular hydrogen bond present in CP, NP and AP. The data regarding structure parameters are compared with corresponding experimental values for 4-hydroxybiphenyl<sup>9</sup> and 4-methoxy-3-nitrophenyl<sup>24</sup> in the same table, as experimental structure is not available for CP, NP and AP. It can be seen from Table 1 that the RMSD values for bond lengths, bond angles and dihedral angles are (0.094 Å,



**Figure 1.** Optimized molecular structure of CP, NP and AP along with numbering of atoms and minimum energy.

0.088 Å and 0.094 Å); (0.722°, 0.786° and 0.823°) and (2.108°, 1.815° and 2.086°) for CP, NP and AP, respectively. From Table 1, it is evident that the theoretical structure parameters for CP, NP and AP are close to their corresponding experimental values in related molecules.<sup>9,24,25,44</sup> For example, as per the calculations made for NP, the average value of intra-ring C–C bond length is 1.396 Å; the mean value of nitro N–O bond is 1.235 Å; inter-ring C–C bond measures 1.484 Å; phenolic C–O bond spans 1.337 Å; and nitro C–N bond is estimated at 1.453 Å. They concur nicely with their corresponding x-ray values for 4-methoxy-3-nitrophenyl<sup>24</sup> near 1.378 Å; 1.212 Å; 1.473 Å; 1.336 Å; and 1.459 Å, respectively. Theoretical value for each C–H bond length is invariably less than their corresponding experimental x-ray values, as listed in Table 1. This systematic deviation is attributable to the inherent inability of x-ray methods to locate exact position of the hydrogen atoms. The reason is, the electron cloud surrounding the hydrogen atom responsible for x-ray scattering is diffuse, as it mainly arises from the sole valence electron of the hydrogen atom resulting in poor scattering and consequent uncertainty in the position of hydrogen atom.

From Table 1, we see that the amino C–N bond length in AP at 1.394 Å is considerably smaller than that of nitro C–N bond length in NP near 1.453 Å. Since, the nitro group, being a deactivating moiety, withdraws electron charge from the ring system, accumulating it across its C–N bond, thereby weakening it due to increased repulsion between the existing electronic charge and presently accumulated negative charge with consequent lengthening of the bond, whereas the amino group, being an activating species, donates lone pair on its nitrogen atom to the ring system decreasing electron density across its C–N bond, which manifests itself in strengthening it, with subsequent shortening of the C–N bond.

There are three angles around carbon atom where nitro group is substituted and three more angles around carbon atom to which hydroxyl moiety is attached, which need to be mentioned here, in NP. These are:  $\angle C8C9C10$ ,  $\angle C8C9N19$ ,  $\angle C10C9N19$ ,  $\angle C9C10C11$ ,  $\angle C9C10O20$ , and  $\angle C11C10O20$  having theoretical values at 121.37°, 117.89°, 120.73°, 117.17°, 124.83°, and 117.99°, respectively (see Figure 1 and Table 1). The experimental x-ray values for their corresponding angles in 4-methoxy-3-nitrobiphenyl are near 121.36°, 116.53°, 121.11°, 116.20°, 124.48°, and 119.30°, respectively. Hence, the theoretical values obtained in the investigation can be considered as in good agreement with experimental values.

Further, the chlorine atom of CN is located in the plane of phenolic ring, whereas deviation of the nitro group of NP from coplanarity with the phenolic ring is insignificant, while the non-coplanarity of the amino group of AP from the phenolic ring plane is significant. This variation resulted is due to the steric repulsion. The amount of steric repulsion exerted on chlorine atom of CP, nitro group of NP, and amino group of AP is the same, as it arises from the same set of nearest hydrogen atom (H18, see Figure 1) and the hydroxyl moiety in the three molecules. This steric repulsive force is perfectly balanced by the chlorine atom of CP, due to its considerable mass, retaining its position in the phenolic ring plane, whereas the nitro group of NP being less in mass in comparison with that of chlorine atom of CP gets slightly displaced from the phenolic ring plane, while the amino group being the lightest of the three substituents (–Cl, –NO<sub>2</sub> and –NH<sub>2</sub>) undergoes significant twist around amino C–N bond in an effort to confer the steric effect effectively.

Present calculations predict formation of intra-molecular hydrogen bond in CP, NP and AP. This bond is manifested between chlorine atom and hydroxyl hydrogen atom in CP; between oxygen atom of the nitro group and adjacent hydroxyl hydrogen atom in NP; and hydroxyl oxygen atom and the nearest hydrogen atom of the amino moiety. The relevant hydrogen bonds are H23...Cl19, H23...O25, and H25...O20 having lengths 2.424 Å, 1.725 Å, and 2.302 Å in CP, NP, and AP, respectively.

## 4.2. Vibrational assignments

Geometry optimization described in Section 3 showed that the molecules of CP, NP and AP were non-planar with C<sub>1</sub> symmetry in the ground state. CP consists of 23 atoms, whereas this number is 25 for NP and AP. Hence, the number of vibrational fundamentals for CP is 63, whereas the same parameter for NP and AP is 69 each, according to the formula (3N-6) for a nonlinear molecule, where N is the number of atoms in the molecule. All these fundamental vibrations in the three molecules with C<sub>1</sub> symmetry belong to a-species and are active in both infrared and Raman spectra.

Observed infrared and Raman frequencies, corresponding un-scaled and scaled frequencies computed by theory, predicated IR and Raman intensities, potential energy distribution (PED) and vibrational assignments for CP, NP and AP are listed in Tables 2–4, respectively. Modes originating from the aromatic nucleus are designated using Wilson's notation,<sup>45</sup> for the phenolic ring substituted with either chlorine atom or nitro group or amino moiety, considering it as a tri-substituted benzene<sup>46</sup> and with a prime (') on the mode for the non-phenolic ring, treating it as a

Table 2. Observed, calculated frequencies (in  $\text{cm}^{-1}$ ) with DFT/6-311++G(d,p) and vibrational assignment of CP.

S. no	Obs. freq. ( $\text{cm}^{-1}$ )			Cal. freq. ( $\text{cm}^{-1}$ )			Intensity <sup>a</sup>		Vibrational assignment <sup>b</sup>	Mode identification <sup>c</sup>
	IR	Raman	(biphenyl) unit	Un-scaled	Scaled	IR (I)	Raman (S <sub>i</sub> )			
1	-	3065		3191	3066	0.921	54.893	98(2')	$\nu(\text{C-H})_2'$	
2	-	3065		3199	3060	4.368	55.118	99(2)	$\nu(\text{C-H})_2$	
3	-	3065		3181	3058	3.091	12.984	96(20a)	$\nu(\text{C-H})_{20a}$	
4	-	3065		3176	3057	9.991	6.529	96(20a')	$\nu(\text{C-H})_{20a}'$	
5	-	3065		3167	3052	2.707	15.464	95(7b')	$\nu(\text{C-H})_{7b}'$	
6	3030	-		3183	3043	4.228	7.385	94(20b')	$\nu(\text{C-H})_{20b}'$	
7	3030	-		3197	3041	0.373	27.180	95(20b)	$\nu(\text{C-H})_{20b}$	
8	3030	-		3161	3037	1.969	4.120	97(7a')	$\nu(\text{C-H})_{7a}'$	
9	-	1608		1645	1610	7.095	34.604	67(8b)+14(18a)+9(6b)	$\nu(\text{C-C})_{8b}$	
10	-	1598		1640	1598	9.135	100.00	63(8a)+17(18b')+11(12')	$\nu(\text{C-C})_{8a}$	
11	-	1598		1604	1589	1.162	1.301	42(8a)+19(8a')+12(18b')+7(12)	$\nu(\text{C-C})_{8a}$	
12	1590	-		1620	1582	4.478	0.506	41(8b')+19(8b)+7(18b')+6(6b)	$\nu(\text{C-C})_{8b}$	
13	1480	-		1539	1464	70.981	12.449	39(18a)+37(19b)+6(18a')+6(13)	$\nu(\text{C-C})_{19b}$	
14	1446	-		1514	1445	20.461	5.368	52(18a')+33(19a')+7(18a)+6(19a)	$\nu(\text{C-C})_{19a}$	
15	1411	-		1480	1416	1.292	1.090	38(18a')+31(19b')+13(19b)+5(15')+5(18a)	$\nu(\text{C-C})_{19b}$	
16	1367	-		1430	1379	1.631	0.867	48(19a)+17(18a)+13(18a')+12(19a')	$\nu(\text{C-C})_{19a}$	
17	-	-		1367	1325	9.543	1.045	68(14)+17( $\beta$ (OH)) + 6(3)	$\nu(\text{C-C})_{14}$	
18	-	1284		1352	1289	0.512	0.882	72(14')+25(3')	$\nu(\text{C-C})_{14}$	
19	1273	-		1322	1267	2.880	0.282	40(3')+23(14')+14(3)+8( $\beta$ (OH)) + 6(14)	$\beta(\text{CH})_{3'}$	
20	-	-		1311	1247	9.053	0.485	33(3)+30(14)+18(14')+12(3')	$\beta(\text{CH})_3$	
21	1225	-		1297	1218	32.617	15.767	31(7a)+26(14)+12(12')+8(14')+6( $\beta$ (OH)) + 6(18a')	$\nu(\text{C-O})_{7a}$	
22	-	1183		1268	1183	4.138	75.969	43(18a)+16(14')+15(14)+10(12)+7(13)	$\beta(\text{CH})_{18a}$	
23	1146	-		1205	1143	1.813	1.323	82(9a')+17(14')	$\beta(\text{CH})_{9a}'$	
24	-	-		1183	1119	0.090	1.323	84(9b')+12(14')	$\beta(\text{CH})_{9b}'$	
25	-	-		1157	1114	2.569	2.908	53(18b)+28(14)	$\beta(\text{CH})_{18b}$	
26	1056	-		1104	1058	2.303	0.044	48(18b')+47(19a')	$\beta(\text{CH})_{18b}'$	
27	-	1046		1066	1044	1.931	2.351	48(12')+32(11)+19(18b)	$\beta(\text{CCC})_{12'}$	
28	-	1023		1058	1023	2.562	0.722	43(11')+27(18a')+25(12')	$\nu(\text{C-C})_{1'}$	
29	-	-		979	1004	5.683	8.042	52(12)+28(11')+13(11)+10(18a')	$\beta(\text{CH})_{18a}'$	
30	-	-		1015	979	5.358	14.793	52(12)+28(11')+13(11)+10(18a')	$\beta(\text{CCC})_{12}$	
31	880	-		1003	876	0.013	0.046	85(5')+15(16b')	$\pi(\text{CH})_{5'}$	
32	-	861		984	867	0.276	0.490	80(17a')+8(16a')+7(5)	$\pi(\text{CH})_{17a}'$	
33	-	861		967	865	0.052	0.203	57(5)+21(4)+9(10b)+8(5')	$\pi(\text{CH})_5$	
34	-	-		891	834	2.124	0.258	49(17b')+15(17b')+14(4)+12(10b)+5(4')	$\pi(\text{CH})_{17b}$	
35	-	-		932	812	5.704	3.702	66(17b')+16(17b)+7(4)+5(4')	$\pi(\text{CH})_{17b}'$	
36	-	-		868	792	4.021	0.371	30(12)+27(7a)+26(1)	$\nu(\text{C-C})_1$	
37	758	-		855	762	5.228	1.115	99(11')	$\pi(\text{CH})_{11}'$	
38	758	-		840	758	0.020	1.428	75(11)+11(16a)+7(10a)	$\pi(\text{CH})_{11}$	

(continued)

Table 2. Continued.

S. no	Obs. freq. (cm <sup>-1</sup> )		Cal. freq. (cm <sup>-1</sup> )		Intensity <sup>a</sup>		Vibrational assignment <sup>b</sup>	Mode identification <sup>c</sup>
	IR	Raman	Un-scaled	Scaled	IR (I)	Raman (S)		
39	-	712	777	713	7.845	4.055	60(4')+16(10a')+10(10b')+6(11)	$\pi(\text{CH})10a'$
40	-	712	748	701	20.555	0.489	50(6b')+11(13)+10(6b)+9(7a)+8(1)+5(18a')	$\nu(\text{C}-\text{C})13$
41	694	687	708	694	6.451	0.060	48(4)+16(4')+12(10a)+10(10b)	$\tau(\text{CCCC})4$
42	-	-	712	658	13.452	0.067	72(17b')+17(4')+5(4)	$\tau(\text{CCCC})4'$
43	-	-	635	643	0.768	1.027	73(6b')+8(6b)	$\beta(\text{CCC})6b'$
44	-	622	694	626	18.550	1.548	65(6b)+10(6b')+6(7b)+6(1)	$\beta(\text{CCC})6b$
45	580	-	601	581	0.611	0.071	34(16b)+24(10a)+16(17a)+10(10a')+9(10b)	$\tau(\text{CCCC})16b$
46	-	-	595	562	10.266	1.074	42(6a')+25(6a')+11(7a)	$\beta(\text{CCC})6a$
47	-	-	543	494	1.548	0.348	30(16b')+18(10b')+17(15)+9(5)+7(6a)	$\tau(\text{CCCC})16b'$
48	-	446	450	438	2.127	0.241	59(16a')+17(17a)+8(17a')	$\tau(\text{CCCC})16a$
49	-	411	494	423	4.959	1.076	32(16a)+15(16a')+12(9b)+10(10a)+9(7b)+5(10b')	$\beta(\text{CO})9b$
50	-	-	417	405	0.254	0.807	83(16a')+16(17b')	$\tau(\text{CCCC})16a'$
51	-	-	433	380	20.709	0.145	20(9b)+17(6b)+15(10a)+9(15')	$\pi(\text{CO})10a$
52	-	301	368	308	1.076	0.512	35(16a')+10(7b)+9(9b)+8(15)+6(16a)+5(10a)	$\beta(\text{C}-\text{C})15$
53	-	247	265	253	0.159	0.326	30(6a')+28(13)+12(6a)+6(1)	$\beta(\text{CCC})6a'$
54	-	-	302	224	0.565	0.650	65(7b)+6(15)+5(9b)	$\nu(\text{C}-\text{Cl})7b$
55	-	-	237	214	0.040	0.678	22(17a)+15(16a)+12(15')+8(16a')+8(9a)+8(11)	$\beta(\text{C}-\text{O})15'$
56	-	180	214	181	0.777	0.204	55(9a)+9(16a')+7(17a)	$\beta(\text{CC})9a$
57	-	150	162	155	0.089	0.640	53(16a)+16(17a)+6(10b)+6( $\tau(\text{C}-\text{C})7$ )	$\pi(\text{CC})17a$
58	-	-	94	89	0.005	0.325	27(15)+22(15')+21(16a)+8(9a)+6(10b')	$\pi(\text{C}-\text{C})10b'$
59	-	74	71	69	0.075	0.547	37(10b')+22(16a)+14(10b)+8(17b)	$\pi(\text{C}-\text{O})10b$
60	-	-	51	44	0.009	1.773	85( $\tau(\text{C}-\text{C})7$ )+5(16a)	$\tau(\text{C}-\text{C})7$
(ii) Vibrations of OH moiety								
61	3346	-	3767	3346	49.318	21.074	100( $\nu(\text{OH})$ )	$\nu(\text{OH})$
62	-	1158	1208	1156	100.00	13.154	36( $\beta(\text{OH})$ )+27(19b)+18(7a)+12(18a')	$\beta(\text{OH})$
63	-	370	409	370	24.668	0.328	86( $\tau(\text{OH})$ )+6(16a)	$\tau(\text{OH})$
RMSD				7.09				

–: Not observed. a: Relative infrared and Raman intensities are normalized to 100. b: Number before the parenthesis is % of PED. Number in the parenthesis is vibrational mode. PED less than 5% is not shown. c: Mode in Wilson's notation,<sup>45</sup> for phenolic ringprime (') on the mode (in Wilson's notation) refers to the modes associated with the non-phenolic ring and  $\nu$ , stretching;  $\beta$ , in-plane bending;  $\pi$ , out-of-plane bending;  $\tau$ , torsion.

Table 3. Observed, calculated frequencies (in  $\text{cm}^{-1}$ ) with DFT/6-311++G(d,p) and vibrational assignment of NP.

S. no	Obs. freq. ( $\text{cm}^{-1}$ )			Cal. freq. ( $\text{cm}^{-1}$ )			Intensity <sup>a</sup>	Vibrational assignment <sup>b</sup>	Mode identification <sup>c</sup>
	IR	Raman	Raman	Un-scaled	Scaled	IR(I)			
(i) Vibrations of aromatic (biphenyl) unit									
1	3069	3061	3061	3193	3071	4.432	82.715	99(2')	$\nu(\text{C-H})_2'$
2	3069	3061	3061	3219	3065	0.676	4.995	98(2)	$\nu(\text{C-H})_2$
3	3069	3061	3061	3177	3062	8.812	7.121	96(20a')	$\nu(\text{C-H})_{20a}'$
4	3069	3061	3061	3168	3055	3.732	18.659	97(7b')	$\nu(\text{C-H})_{7b}'$
5	3069	3061	3061	3281	3048	0.254	39.627	98(20a)	$\nu(\text{C-H})_{20a}$
6	3035	—	—	3184	3047	0.254	15.950	96(20b')	$\nu(\text{C-H})_{20b}'$
7	3035	—	—	3163	3042	1.205	3.613	98(7a')	$\nu(\text{C-H})_{7a}'$
8	3035	—	—	3201	3026	1.518	11.789	98(20b)	$\nu(\text{C-H})_{20b}$
9	1630	1634	1634	1667	1640	30.608	33.497	63(8b)+14(18a)+9(6b)	$\nu(\text{C-C})_{8b}$
10	—	1582	1582	1642	1606	5.540	83.915	65(8a')+20(18b')+10(12')	$\nu(\text{C-C})_{8a}$
11	1577	—	—	1620	1585	2.690	4.596	62(8b')+16(18b')+9(12')+7(8b)	$\nu(\text{C-C})_{8b}'$
12	—	1582	1582	1609	1566	1.907	12.001	55(8a)+9[ $\nu_{as}(\text{NO}_2)$ ]+8(18a)+7(6b)+6(8a')	$\nu(\text{C-C})_{8a}$
13	—	1499	1499	1514	1494	43.059	19.848	31(19b)+29(18a)+12(7a)+9(18a')+6(19b')	$\nu(\text{C-C})_{19b}$
14	1475	—	—	1536	1476	33.350	1.635	52(18a')+28(19b')+8(18a)+7(19b)	$\nu(\text{C-C})_{19b}'$
15	1450	1449	1449	1481	1437	9.594	1.584	46(18b')+32(19a')+7(19a)	$\nu(\text{C-C})_{19a}'$
16	1408	1408	1408	1443	1408	8.799	7.249	57(19a)+15(18a)+7(18a')+6(19a')	$\nu(\text{C-C})_{19a}$
17	1322	—	—	1360	1324	59.213	4.417	25(14')+16(14)+16[ $\nu_s(\text{NO}_2)$ ]+14(3)+11(7a)	$\nu(\text{C-C})_{14}$
18	1322	—	—	1349	1321	7.987	1.057	46(14')+46(3')	$\nu(\text{C-C})_{14}'$
19	—	1283	1283	1323	1287	10.088	1.629	50(14')+28(3')+7(14)	$\beta(\text{CH})_3'$
20	—	1283	1283	1306	1272	45.366	17.024	38(3)+23[ $\beta(\text{OH})$ ]+9[ $\nu_s(\text{NO}_2)$ ]+7(7b)+6(14)	$\beta(\text{CH})_3$
21	1247	—	—	1273	1249	63.073	17.038	27(18a)+23(7a)+18[ $\nu_s(\text{NO}_2)$ ]+7(18a)	$\nu(\text{C-O})_{7a}$
22	—	1230	1230	1304	1226	13.143	100.00	32(13)+17(18a)+9(12)+8(14)+8(12')+7(7b)	$\beta(\text{CH})_{18a}$
23	—	1154	1154	1207	1170	11.785	1.713	66(9a')+16(14')+9(18a)	$\beta(\text{CH})_{9a}'$
24	—	1132	1132	1184	1148	0.075	1.226	84(9b')+16(14')	$\beta(\text{CH})_{9b}'$
25	1136	—	—	1162	1135	15.313	6.206	40(18b)+23(14)+14(7b)+5[ $\beta(\text{OH})$ ]	$\beta(\text{CH})_{18b}$
26	1076	—	—	1101	1077	2.953	2.209	23(12)+18(19b)+12(7b)+9(19b')+8(18b)	$\nu(\text{C-N})_{7b}$
27	1076	—	—	1106	1073	0.763	0.427	42(19b')+33(18b')+6(12)+6(19b)	$\beta(\text{CH})_{18b}'$
28	—	1044	1044	1067	1046	1.576	3.696	35(1)+22(1')+17(18a)+12(18a')+10(12')	$\nu(\text{C-C})_1$
29	1037	—	—	1041	1024	1.358	0.539	41(12')+39(1')+13(18a')	$\beta(\text{CCC})_{12}'$
30	—	995	995	1015	1000	0.030	21.686	60(1')+35(12')	$\nu(\text{C-C})_1'$
31	919	—	—	989	911	0.249	0.639	84(5)+14(16b)	$\pi(\text{CH})_5$
32	919	—	—	1005	905	0.007	0.027	87(5')+13(16a')	$\pi(\text{CH})_5'$
33	—	—	—	985	897	0.082	0.167	90(17a')+9(4')	$\pi(\text{CH})_{17a}'$
34	888	—	—	912	888	1.489	0.994	39(12)+20[ $\delta(\text{NO}_2)$ ]+9[ $\nu_s(\text{NO}_2)$ ]+6(1')+6(7b)	$\beta(\text{CCC})_{12}$
35	860	—	—	919	862	1.275	0.028	40(17b)+25(17b')+17(16b)+7(16b')+5(10b)	$\pi(\text{CH})_{17b}$
36	860	—	—	938	846	2.092	0.208	48(17b')+33(17b)+11(4)+5(4')	$\pi(\text{CH})_{17b}'$
37	—	—	—	856	793	0.081	2.168	99(11')	$\pi(\text{CH})_{11}'$
38	—	—	—	852	786	2.553	0.886	67(11)+11(16a)+8(10b)+6(16a')	$\pi(\text{CH})_{11}$

(continued)

Table 3. Continued.

S. no	Obs. freq. (cm <sup>-1</sup> )		Cal. freq. (cm <sup>-1</sup> )		Intensity <sup>a</sup>		Vibrational assignment <sup>b</sup>	Mode identification <sup>c</sup>
	IR	Raman	Un-scaled	Scaled	IR(I)	Raman(S)		
39	763	-	779	760	3.072	0.272	64(16a')+17(10a')+11(17a')	$\pi(\text{CH})10a'$
40	-	740	753	728	2.371	2.958	20(12')+14(12)+10( $\delta(\text{NO}_2)$ )+10(13)	$\nu(\text{C}-\text{C})13$
41	-	-	740	722	17.852	0.230	64(4)+11(11)+10(10a')+5(10b)	$\tau(\text{CCCC})4$
42	-	-	711	689	12.669	0.127	68(17b')+19(4')	$\tau(\text{CCCC})4'$
43	698	-	695	674	6.217	0.793	35(12)+22(12')+12(18a')	$\beta(\text{CH})18a'$
44	-	617	634	628	0.152	1.016	86(6b')+6(1')+5(18a')	$\beta(\text{CCC})6b'$
45	-	-	601	421	5.544	1.022	28(6b)+27(9b)+15(7b)+6(16b')	$\beta(\text{CCC})6b$
46	-	-	586	541	1.879	0.269	22(16b)+20(16b')+14(10b')+11(10b)+8(17a')+8(10a)	$\tau(\text{CCCC})16b'$
47	500	-	512	493	6.971	0.144	29(16b)+17(16b')+14(10a)+7(10b)+7(10b')	$\tau(\text{CCCC})16b$
48	-	424	437	424	0.169	0.744	72(16a)+19(17a')+8(11)	$\tau(\text{CCCC})16a$
49	575	-	429	573	0.124	1.214	48(6a)+30(6a')	$\beta(\text{CCC})6a$
50	-	402	415	406	0.125	0.921	81(16a')+16(17a')	$\tau(\text{CCCC})16a'$
51	-	-	438	399	1.744	0.484	17(9b)+16(16a)+14(10a)+10(15)+10(15')	$\beta(\text{CO})9b$
52	-	325	370	340	1.487	0.268	28(10a)+20(9b)+10(16a)+8(16a')+8(15')+7(6a)	$\beta(\text{C}-\text{C})15'$
53	-	292	336	301	1.047	0.510	30(16a')+13(9b)+13(10a)+11(15)+6(9a)	$\beta(\text{C}-\text{C})15$
54	-	-	285	267	0.006	0.428	30(6a)+30(13)+16(6a')+8(19b)+5(19b')	$\beta(\text{CCC})6a'$
55	-	-	208	204	0.601	0.387	21(10a)+17(10b)+15(15')+13(16a)+11(9a)+6(11)	$\pi(\text{C}-\text{O})10a$
56	-	178	246	177	0.922	0.445	61(9a)+11(16a')	$\beta(\text{CN})9a$
57	-	-	151	143	0.067	1.070	45(17a)+22( $\tau(\text{OH})$ )+14(16a)+7( $\tau(\text{C}-\text{C})$ )	$\pi(\text{C}-\text{N})17a$
58	-	70	84	78	0.162	0.239	21(15)+19( $\tau(\text{NO}_2)$ )+17(10b')+12(9a)+5(16a')	$\pi(\text{C}-\text{C})10b'$
59	-	-	58	57	0.008	0.325	49( $\tau(\text{NO}_2)$ )+17(16a)+10( $\tau(\text{OH})$ )+9(10b)+5(10b')	$\pi(\text{C}-\text{C})10b$
60	-	-	48	46	0.098	1.682	70( $\tau(\text{C}-\text{C})$ )+12( $\tau(\text{NO}_2)$ )+6(16a)	$\tau(\text{C}-\text{C})$
(ii) Vibrations of OH moiety								
61	3450	-	3472	3450	90.490	38.663	100( $\nu(\text{OH})$ )	$\nu(\text{OH})$
62	1170	-	1230	1177	53.823	5.743	41(18a)+21( $\beta(\text{OH})$ )+12(19b)+11(18a')	$\beta(\text{OH})$
63	668	-	703	669	33.657	0.167	63( $\tau(\text{OH})$ )+19(16b)+8(11')+5(10b)	$\tau(\text{OH})$
(iii) Vibrations of nitro group								
64	1538	1541	1578	1540	100.00	14.537	55( $\nu_{as}(\text{NO}_2)$ )+17(19a)+6( $\nu(\text{NO}_2)$ )	$\nu_{as}(\text{NO}_2)$
65	1371	-	1410	1372	30.596	33.895	53(19b)+13( $\beta(\text{OH})$ )+10( $\nu_s(\text{NO}_2)$ )+10(7b)	$\nu_s(\text{NO}_2)$
66	-	822	840	825	2.148	10.687	32( $\delta(\text{NO}_2)$ )+29(1)+16(12)+11(7a)	$\delta(\text{NO}_2)$
67	639	-	714	639	3.786	0.129	57( $\omega(\text{NO}_2)$ )+10(17a)+16(4)	$\omega(\text{NO}_2)$
68	560	-	576	557	2.346	1.056	53( $\tau(\text{NO}_2)$ )+11(1)+10(9b)+7(9a)	$\gamma(\text{NO}_2)$
69	-	-	93	87	0.117	0.134	34( $\tau(\text{NO}_2)$ )+15( $\tau(\text{OH})$ )+12(10b)+1(15')+6(15)	$\tau(\text{NO}_2)$
RMSD				9.39				

-: Not observed. a: Relative infrared and Raman intensities are normalized to 100. b: Number before the parenthesis is % of PED. Number in the parenthesis is vibrational mode. PED less than 5% is not shown. c: Mode in Wilson's notation,<sup>45</sup> for phenolic ring prime(') on the mode (in Wilson's notation) refers to the modes associated with the non-phenolic ring and  $\nu$ , stretching;  $\beta$ , in-plane bending;  $\pi$ , out-of-plane bending;  $\delta$ , scissoring;  $\delta$ , scissoring;  $\gamma$ , rocking;  $\omega$ , wagging;  $\tau$ , torsion; s, symmetric; as, asymmetric.



Table 4. Observed, calculated frequencies (in  $\text{cm}^{-1}$ ) with DFT/6-311++G(d,p) and vibrational assignment of AP.

S. no	Obs. freq. ( $\text{cm}^{-1}$ )		Cal. freq. ( $\text{cm}^{-1}$ )		IR (I)	Raman (S)	Intensity <sup>a</sup>	Vibrational assignment <sup>b</sup>	Mode identification <sup>c</sup>
	IR	Raman	Un-scaled	Scaled					
(i) Vibrations of aromatic (biphenyl) unit									
1	–	3059	3188	3070	2.509	15.344	97(2)	$\nu(\text{C-H})_2$	
2	–	3059	3190	3063	7.682	58.836	98(2')	$\nu(\text{C-H})_2$	
3	–	3059	3176	3055	15.754	3.433	96(20a')	$\nu(\text{C-H})_{20a'}$	
4	–	3059	3166	3050	4.547	8.670	97(7b')	$\nu(\text{C-H})_{7b'}$	
5	–	3059	3147	3046	5.149	8.494	98(20a)	$\nu(\text{C-H})_{20a}$	
6	3030	–	3181	3039	2.059	19.940	96(20b')	$\nu(\text{C-H})_{20b'}$	
7	3030	–	3159	3032	9.596	21.320	98(7a')	$\nu(\text{C-H})_{7a'}$	
8	3030	–	3163	3030	5.368	3.987	98(20b)	$\nu(\text{C-H})_{20b}$	
9	–	1599	1642	1596	12.044	0.891	68(8b') + 18(18b') + 11(12')	$\nu(\text{C-C})_{8b'}$	
10	–	1599	1638	1587	40.492	100.00	70(8a') + 17(18b') + 10(12')	$\nu(\text{C-C})_{8a'}$	
11	1525	1528	1612	1536	0.847	3.146	59(8b) + 15(18a) + 11(6b)	$\nu(\text{C-C})_{8b}$	
12	1525	1528	1633	1526	26.158	4.969	52(8a) + 9(6b) + 6(18a)	$\nu(\text{C-C})_{8a}$	
13	–	1494	1552	1486	65.771	16.598	34(18a') + 27(19b') + 12(19b) + 12(13) + 8(18a)	$\nu(\text{C-C})_{19b'}$	
14	1476	1461	1522	1461	73.360	3.461	30(19b) + 26(18a) + 17(18a') + 10(19b') + 8(7a)	$\nu(\text{C-C})_{19b}$	
15	–	1413	1485	1420	8.701	8.302	43(18b') + 31(19a') + 9(19a)	$\nu(\text{C-C})_{19a'}$	
16	1400	–	1456	1393	9.288	3.587	30(19a) + 15(18a') + 14(19a') + 10(18a) + 8(7b)	$\nu(\text{C-C})_{19a}$	
17	–	1312	1351	1316	43.817	20.169	76(14') + 16(3')	$\nu(\text{C-C})_{14'}$	
18	1301	–	1372	1300	7.881	5.128	32(14) + 22(3) + 9[\beta(\text{OH})] + 8(13) + 8(7a) + 7(7b)	$\nu(\text{C-C})_{14}$	
19	–	–	1339	1277	11.873	13.257	27(3') + 14(14) + 13(14') + 10[\gamma(\text{NH}_2)] + 10(3) + 6(13)	$\beta(\text{CH})_{3'}$	
20	–	–	1333	1272	13.185	5.253	40(14) + 30(3) + 10[\beta(\text{OH})] + 6(13) + 6(3')	$\beta(\text{CH})_3$	
21	1251	1250	1277	1254	13.185	5.253	21(19b') + 17(18a) + 16(18a') + 16(19b) + 10(7a)	$\nu(\text{C-O})_{7a}$	
22	–	–	1302	1234	11.663	2.984	31(14) + 25(18a) + 19(7a) + 7(13)	$\beta(\text{CH})_{18a}$	
23	1194	–	1242	1201	9.729	3.018	23(7b) + 22(18a) + 11(7a) + 11(12) + 9(13) + 5[\beta(\text{OH})]	$\nu(\text{C-N})_{7b}$	
24	1155	1159	1204	1159	0.029	1.975	83(9a') + 16(14')	$\beta(\text{CH})_{9a'}$	
25	–	–	1181	1135	0.013	1.051	88(9b') + 12(14')	$\beta(\text{CH})_{9b'}$	
26	1067	–	1100	1063	3.121	0.008	50(19b') + 44(18b')	$\beta(\text{CH})_{18b'}$	
27	–	–	1104	1050	81.161	0.141	30(14) + 21(18b) + 13[\gamma(\text{NH}_2)] + 8(12) + 5[\beta(\text{OH})]	$\beta(\text{CH})_{18b}$	
28	1032	–	1060	1033	0.032	7.349	55(1') + 28(18a') + 13(12')	$\beta(\text{CH})_{18a'}$	
29	–	–	1040	1019	3.680	1.774	66(12') + 19(1') + 7(1)	$\beta(\text{CCCC})_{12'}$	
30	–	–	1015	994	1.267	9.671	39(1') + 38(1) + 10(18a') + 8[\gamma(\text{NH}_2)]	$\nu(\text{C-C})_{1'}$	
31	–	997	1000	968	0.239	0.068	80(5') + 20(16b')	$\pi(\text{CH})_{5'}$	
32	927	–	983	945	0.090	0.344	90(17a') + 9(4')	$\pi(\text{CH})_{17a'}$	
33	–	917	933	916	1.423	0.179	56(17b') + 20(16b') + 12(10b')	$\pi(\text{CH})_{17b'}$	
34	884	–	921	876	2.911	2.312	43(12) + 11(1') + 9(1) + 8(7b) + 7(17b) + 6(13)	$\beta(\text{CCCC})_{12}$	
35	–	839	918	841	0.493	0.183	78(5) + 16(16a)	$\pi(\text{CH})_5$	
36	–	–	855	827	7.166	0.206	99(11')	$\pi(\text{CH})_{11'}$	
37	821	–	878	823	0.012	0.976	33(17b) + 17(4) + 14(4') + 14(17b') + 10(10b) + 9(10b')	$\pi(\text{CH})_{17b}$	
38	–	–	809	790	2.816	1.029	41(17b) + 17(16a') + 14(16a) + 9(10a') + 8(10b')	$\pi(\text{CH})_{10a'}$	

(continued)

Table 4. Continued.

S. no	Obs. freq. (cm <sup>-1</sup> )		Cal. freq. (cm <sup>-1</sup> )		Intensity <sup>a</sup>		Vibrational assignment <sup>b</sup>	Mode identification <sup>c</sup>
	IR	Raman	Un-scaled	Scaled	IR (I)	Raman (S)		
39	758	-	788	748	2.732	5.993	33 (1)+19(11)+12(7a)+10(16a)+10(12)+6(10b)	$\nu$ (C-C1)
40	-	-	771	741	34.030	0.762	46(11)+19(16a')+9(16a)+8(1)+6(10b)	$\pi$ (CH)11
41	-	728	736	719	8.011	0.190	48(4)+18(11)+9(10a)+9(4')+7(17b)	$\tau$ (CCCC)4
42	-	706	711	709	0.987	2.061	49(17b')+23(4)+17(4')	$\tau$ (CCCC)4'
43	696	-	721	700	20.349	0.135	45(12')+22(12)+8(1)+7(13)+7(1')	$\nu$ (C-C7)13
44	625	-	649	636	0.148	0.641	87(6b')+5(18a')	$\beta$ (CCCC)6b'
45	-	600	631	601	10.941	0.073	26(16b)+16(17a)+13(16b')+11(17a')+10(10b)	$\tau$ (CCCC)6b
46	584	-	585	577	16.502	0.765	51(6a)+28(6a')+6(1)	$\beta$ (CCCC)6a
47	-	-	591	562	10.882	0.994	21(16b)+12(17a)+10(10a)+9(15)+8(9b)+8(16b')	$\beta$ (CO)9b
48	-	-	529	538	22.347	0.081	51( $\omega$ (NH <sub>2</sub> ))+10(6a)+10(16b')+6(10b')	$\tau$ (CCCC)6b'
49	452	-	490	452	8.056	0.298	32(16b)+17(6b)+10(17a)+7(16a')+7(9a)+5(15)	$\beta$ (CCCC)6b
50	428	-	450	437	5.489	0.079	34(16a)+31(16a')+6(17a)	$\tau$ (CCCC)6a
51	428	-	417	434	0.105	0.481	60(16a')+18(16a)+6(17b')	$\tau$ (CCCC)6a'
52	-	-	395	325	5.727	0.320	34[ $\tau$ (NH <sub>2</sub> )]+22(10a)+8(15')+5(15)	$\pi$ (CO)10a
53	-	-	306	298	1.841	0.317	34(9a)+25(16a')+10(15)+7(1)	$\beta$ (C-C7)15
54	-	-	321	291	9.083	0.081	29(9a)+25(6a)+10(9b)+8(16a')	$\beta$ (CN)9a
55	-	270	278	265	2.859	0.989	18(9a)+18(13)+16(6a)+13(6a')+12(1)+5(16a')	$\beta$ (CCCC)6a'
56	-	-	236	218	15.112	0.474	26(17a)+24(16a)+12[ $\tau$ (OH)]+12(17b)+8(16a')+6(10a)	$\pi$ (C-N)17a
57	-	171	182	172	0.579	0.332	53(16a)+11(16a')+10(15')+6(10a)	$\beta$ (C7-C)15'
58	-	87	102	93	0.133	0.428	33(15')+20(15)+16(16a')+15(10b')	$\pi$ (C-C7)10b'
59	-	-	72	69	0.656	0.145	27(15')+24(16a)+23(10b)+9(10(10b')+9(17b)	$\pi$ (C7-C)10b
60	-	-	56	54	0.063	1.465	85[ $\tau$ (C-C7)]+5(16a)	$\tau$ (C-C7)
(ii) Vibrations of OH moiety								
61	3469	-	3847	3469	48.282	28.274	100[ $\nu$ (OH)]	$\nu$ (OH)
62	1106	-	1183	1114	29.314	0.347	50(18b)+22(19b)+20[ $\beta$ (OH)]	$\beta$ (OH)
63	-	-	260	254	43.532	0.098	77 [ $\tau$ (OH)]	$\tau$ (OH)
(iii) Vibrations of amino group								
64	3373	-	3672	3373	14.605	8.003	100[ $\nu_{as}$ (NH <sub>2</sub> )]	$\nu_{as}$ (NH <sub>2</sub> )
65	3287	-	3570	3287	16.983	36.465	100 [ $\nu_s$ (NH <sub>2</sub> )]	$\nu_s$ (NH <sub>2</sub> )
66	1602	-	1659	1601	56.310	2.926	88[ $\delta$ (NH <sub>2</sub> )]+7(7b)	$\delta$ (NH <sub>2</sub> )
67	-	1101	1146	1089	2.457	0.517	32(14)+27[ $\beta$ (OH)]+25[ $\gamma$ (NH <sub>2</sub> )]+9(18b)	$\gamma$ (NH <sub>2</sub> )
68	511	-	564	509	100.00	0.615	27( $\omega$ (NH <sub>2</sub> ))+14(6a)+11(16b)+9(7b)+9(16b')+7(10a)	$\omega$ (NH <sub>2</sub> )
69	-	344	342	346	9.082	0.477	47 [ $\tau$ (NH <sub>2</sub> )]+23(10a)+7(16a)+5(16a')+5(17a)	$\tau$ (NH <sub>2</sub> )
RMSD								

–: Not observed. a: Relative infrared and Raman intensities are normalized to 100. b: Number before the parenthesis is % of PED. Number in the parenthesis is vibrational mode. PED less than 5% is not shown. c: Mode in Wilson's notation,<sup>45</sup> for phenolic ring prime(!) on the mode (in Wilson's notation) refers to the modes associated with the non-phenolic ring and  $\nu$ , stretching;  $\beta$ , in-plane bending;  $\pi$ , out-of-plane bending;  $\delta$ , scissoring;  $\gamma$ , rocking;  $\omega$ , wagging;  $\tau$ , torsion; s, symmetric; as, asymmetric.

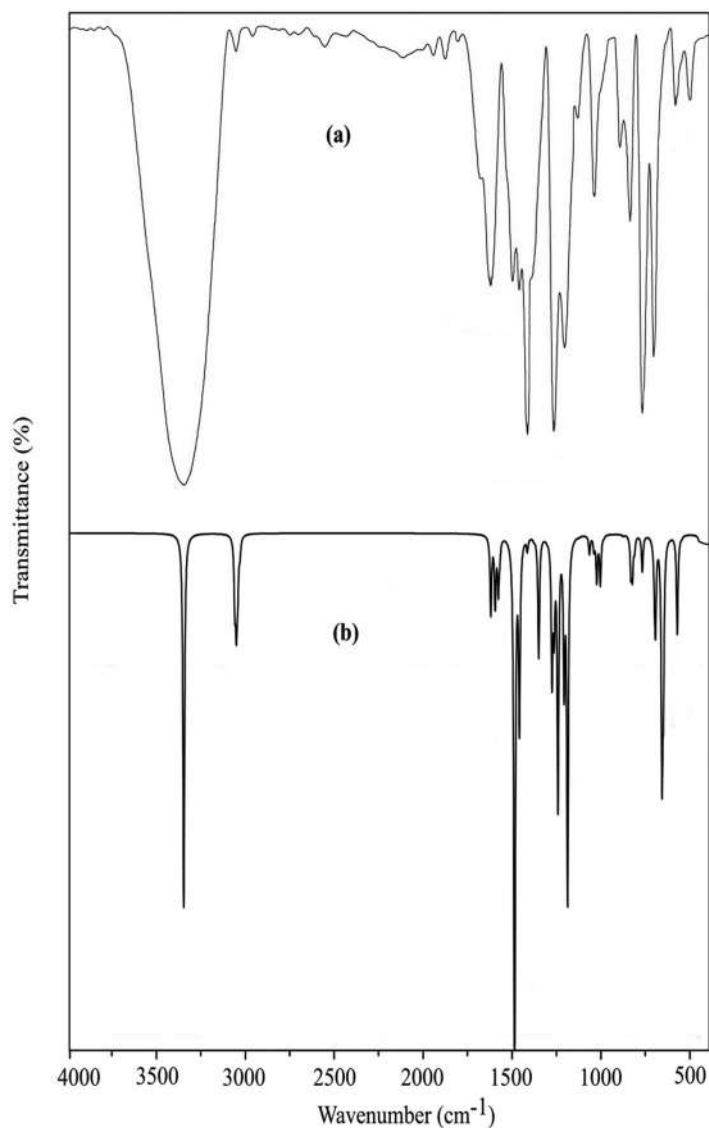


**Figure 2.** FT-IR spectra of CP (a) experimental and (b) simulated with DFT/B3LYP/6-311++G(d,p) formalism.

mono-substituted benzene.<sup>46</sup> A comparison of FT-IR spectra, both experimental and simulated, is made in [Figures 2, 4 and 6](#), for CP, NP and AP, whereas comparison for their Raman counterpart is made in [Figure 3, 5 and 7](#).

The rms error, for CP, NP and AP is 7.44, 8.98 and 6.97  $\text{cm}^{-1}$ , between measured and scaled fundamentals, respectively, whereas the corresponding RMSD values are 7.09, 9.39 and 6.59  $\text{cm}^{-1}$ . Further, observed IR and Raman fundamentals exhibit good agreement with their corresponding computed values, as evident from [Tables 2–4](#) and [Figures 2–7](#) for CP, NP and AP. Hence, reliable vibrational assignments can be proposed for CP, NP and AP, on the basis of present calculations, with emphasis on dominant PED contributions.

The results available in [Tables 2–4](#) are self-explanatory. Hence, the discussion of vibrational assignments is mainly confined to the fundamentals originating from the phenolic ring and its substituents.

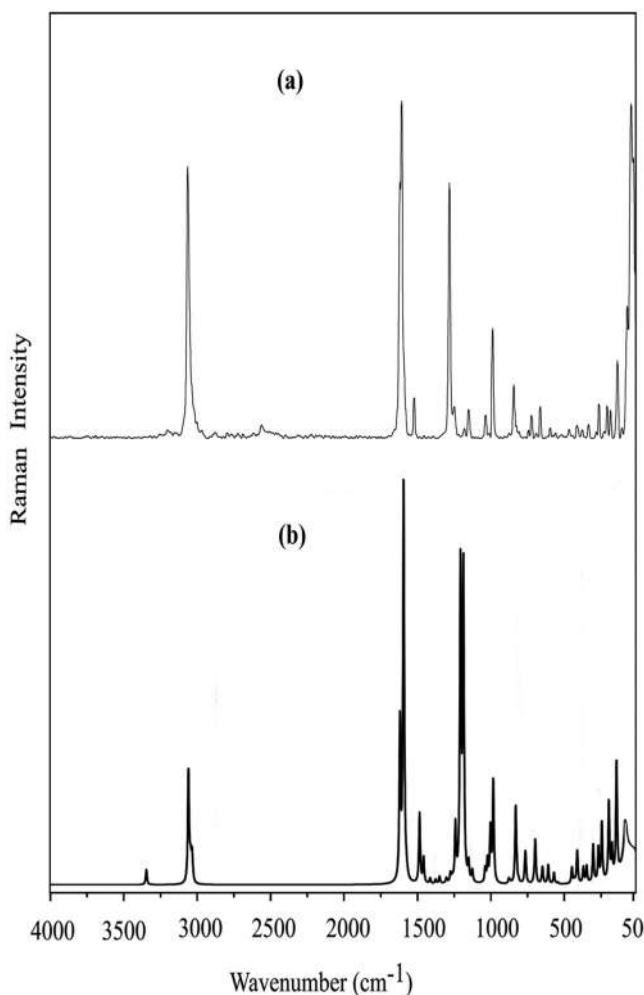


**Figure 3.** FT Raman spectra of CP (a) experimental and (b) simulated with DFT/B3LYP/6-311++G(d,p) formalism.

#### 4.2.1. Vibrations of the phenolic ring

**4.2.1.1. C–C Stretching vibrations:** In CP, NP and AP, modes 8a and 8b are expected in the frequency range  $1500\text{--}1600\text{ cm}^{-1}$ . The higher frequency (scaled value) is a C–C stretching mode to the extent of 59 to 67% in the three molecules. It mixes with C–H in plane bending mode 18a and  $\angle$ CCC bending vibration 6b uniformly in the molecules under consideration. The lower frequency exhibits considerable C–C stretching character ranging from 42 to 55%. It mixes with C–H in-plane bending fundamental 18a and  $\angle$ CCC bending mode 6b in NP and AP to a small extent. It is interesting to note that contributions from 18a and 6b in NP and AP, are replaced by that from mode 18b' (C–H in-plane bending of benzene ring connected to phenolic ring) and  $\angle$ CCC ring bending vibration 12 in CP. It is to be noted that C–C stretching fundamental 8a' of the monosubstituted benzene ring makes a PED contribution of 19% in CP, whereas this component decreases to 6% in NP, while such contribution disappears in AP. There is an additional contribution to this mode from asymmetric stretching vibration of the nitro group in NP. Present computation reveal that the frequency of mode 8b should be higher than that of vibration 8a, which does not agree with that for biphenylcarboxaldehydes, wherein 8a is greater than 8b.<sup>47</sup> Hence, Raman shifts at  $1598$  and  $1582\text{ cm}^{-1}$  in CP and NP, respectively, along with IR absorption

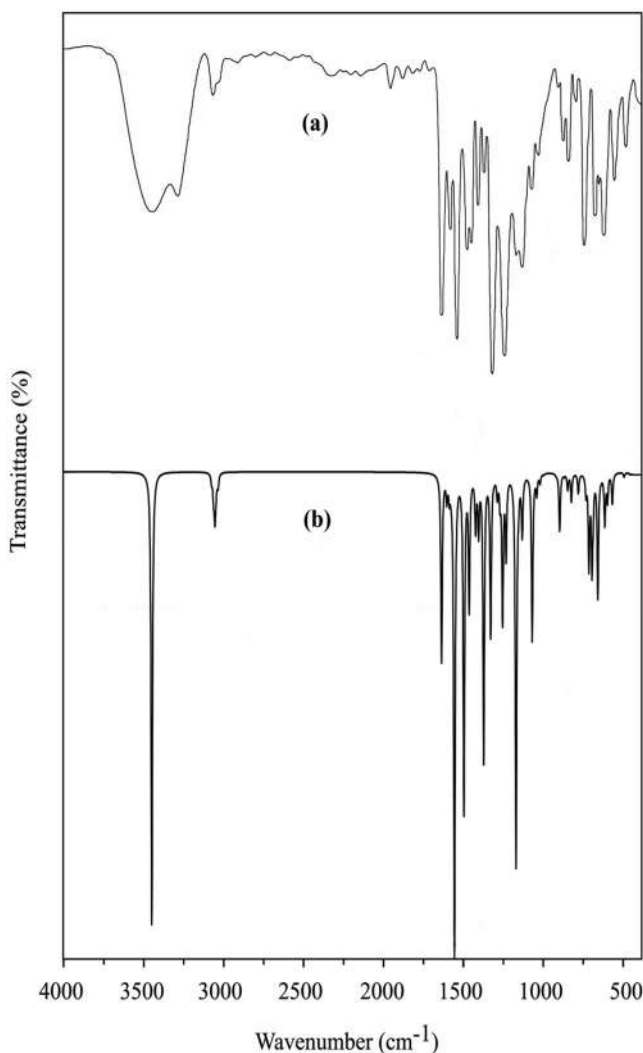


**Figure 4.** FT-IR spectra of NP (a) experimental and (b) simulated with DFT/B3LYP/6-311++G(d,p) formalism.

near  $1525\text{ cm}^{-1}$  are assigned to mode 8a, whereas those around  $1608\text{ R}$  (R indicates Raman shift),  $1630$ , and  $1525\text{ cm}^{-1}$  are ascribed to vibration 8b in CP, NP and AP, respectively.

Modes 19a and 19b normally appear in the spectral region  $1400\text{--}1500\text{ cm}^{-1}$  in benzene derivatives. The C–C stretching character of the higher fundamental falls in the range 30–37% in CP, NP and AP. It mixes strongly with C–H in-plane bending normal frequency in the three molecules. This mode also combines with C–H in-plane bending vibration 18a' in the three molecules. Mixing with other modes can be identified in Tables 2–4 for CP, NP and AP, respectively. Lower frequency exhibits C–C stretching nature to the extent of 30–57%. It mixes with C–H in-plane bending vibration 18a and its counterpart 18a' of the monosubstituted benzene ring. Other minor contributions are available in Tables 2–4 for this mode. According to the present calculations frequency of vibration 19b should be greater than that of mode 19a, which is in direct contradiction with that obtained for biphenylcarboxaldehydes, wherein frequency of 19a is greater than that of 19b.<sup>47</sup> Thus, the IR bands around  $1367$ ,  $1408$  and  $1400\text{ cm}^{-1}$  are attributed to mode 19a, whereas

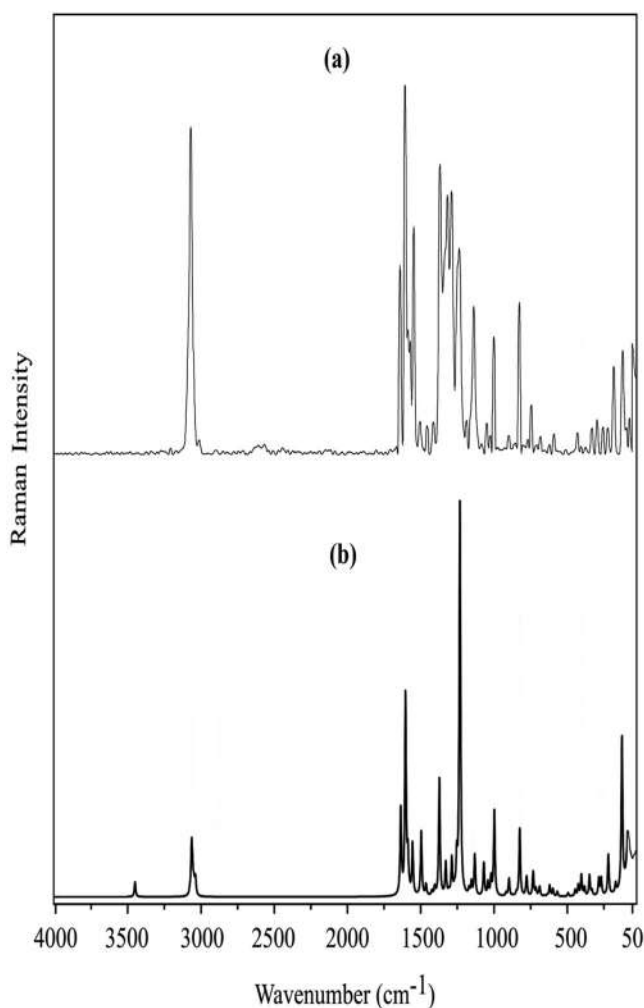


**Figure 5.** FT Raman spectra of NP (a) experimental and (b) simulated with DFT/B3LYP/6-311++G(d,p) formalism.

those near 1480, 1499 R and  $1476\text{ cm}^{-1}$  are assigned to vibration 19b in CP, NP and AP, respectively.

Characteristic feature of vibration 14 is that the alternate carbon bonds of the ring either increase or decrease. It appears at 1325 C (C indicates calculated scaled value), 1322 and  $1301\text{ cm}^{-1}$  in CP, NP and AP, respectively, wherein the C–C stretching character varies from 16% to 68%. It is known that this vibration shows strong mixing with C–H in-plane bending mode 3 in many substituted benzenes. However, this is not valid for present molecules as the corresponding PED contribution from mode 3 is 6% in CP, 14% in NP and 22% in AP. This result is identical with that obtained for biphenylcarboxaldehydes.<sup>47</sup> A note-worthy point is that this fundamental mixes with symmetric stretching of nitro group in NP.

**4.2.1.2. C–H in-plane bending vibrations.** According to the present computations, the bands in the vicinity of 1247 C, 1283 R and  $1272\text{ C cm}^{-1}$  essentially originate from C–H in-plane bending mode 3, as it draws PED to the extent of 33%, 38% and 30% from its own coordinate in CP, NP and AP, respectively. It exhibits significant mixing with C–C stretching vibration 14 in CP and

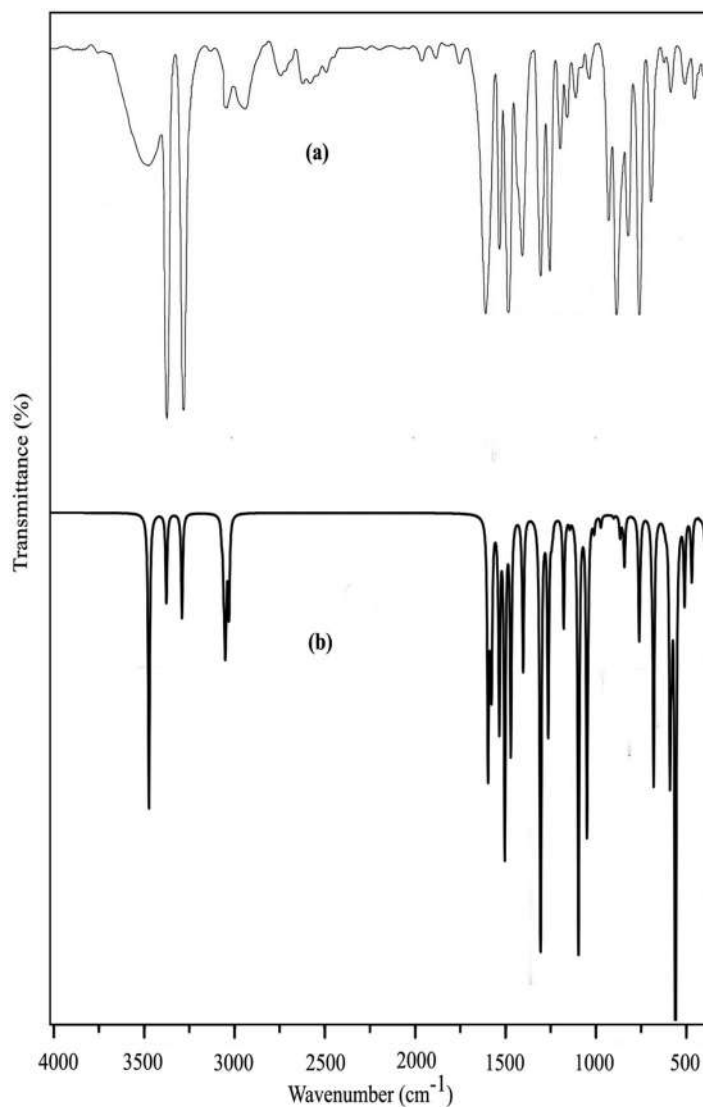


**Figure 6.** FT-IR spectra of AP (a) experimental and (b) simulated with DFT/B3LYP/6-311++G(d,p) formalism.

AP, whereas this mixing is of no significance in NP, as it is very low. This mixing in CP and AP agrees with that for the corresponding vibration in biphenylcarboxaldehydes.<sup>47</sup>

Raman shifts around 1183 and 1230  $\text{cm}^{-1}$  in CP and NP, along with scaled value near 1234  $\text{cm}^{-1}$  in AP are attributed to mode 18a, considering their PED, which is 43%, 17% and 25% in CP, NP and AP, respectively. Strong mixing of this mode with vibrations 13 and 14 in NP and AP, respectively, to the extent of 32% and 31%, is note-worthy, whereas the same mixing drops to 15% in CP. It is important to note that, this vibration mixes with C–O stretching mode 7a with 19% PED in AP. Vibration 18b is predicated at 1114 C, 1136 and 1041 R  $\text{cm}^{-1}$  in CP, NP and AP, respectively, according to the computations. This vibration has strong mixing with mode 14 in the three molecules. Further, its mixing with C–N stretching mode 7b in NP, and the rocking vibration of amino group in AP are important.



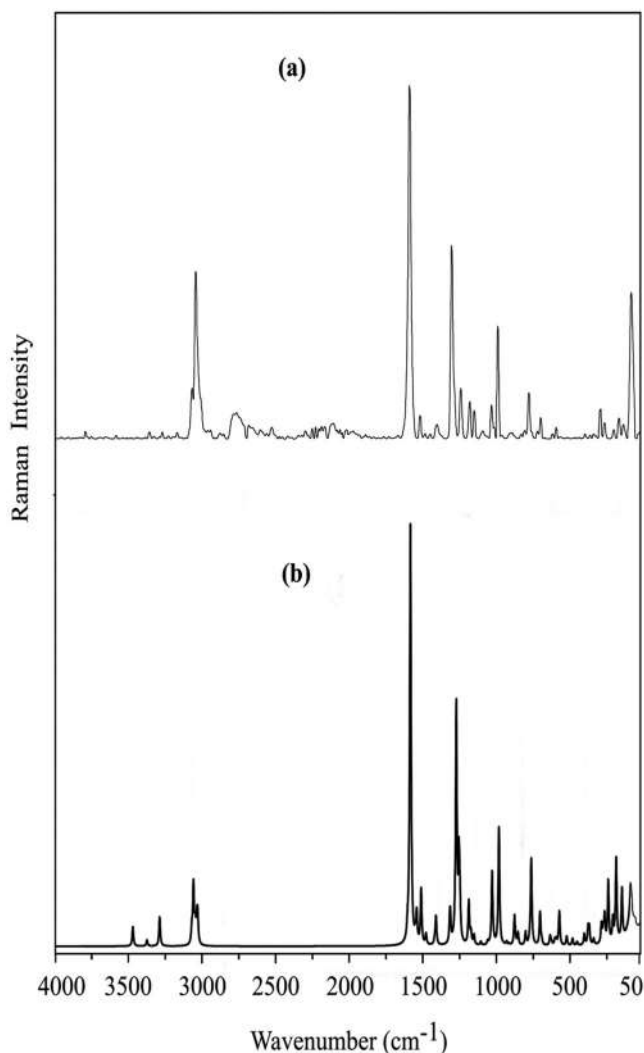


**Figure 7.** FT Raman spectra of AP (a) experimental and (b) simulated with DFT/B3LYP/6-311++G(d,p) formalism.

**4.2.1.3. Ring or substituent sensitive modes.** Vibrations 1, 6a, 6b and 12 are known as ring modes or substituent sensitive modes, as their frequency value varies from molecule to molecule. Further, they are known to mix with several other vibrations of the ring system and substituent group vibrations that share the same complicated region of spectral space. Hence, it is essential to use their characteristic eigenvector distribution carefully, for their correct identification and assignment, as proposed by Patel et al.,<sup>48</sup> and successfully implemented by us for a host of substituted benzenes (for instance see reference<sup>47</sup>). We employed local symmetry coordinates constructed in terms of primitive internal coordinates for vibrations 6a, 6b and 12. Therefore, it is expected that for a given vibration say 12, the corresponding eigenvector element should have a relatively prominent magnitude with respect to the elements of the other two normal frequencies. This is, in fact, found true for the mode 12, wherein the corresponding elements 0.512, 0.639 and 0.602, for CP, NP and AP, respectively, dominate the other two elements ranging from  $-0.005$  to  $0.239$ . Thus the frequencies at  $979$  C,  $888$  and  $884$   $\text{cm}^{-1}$  are assigned to vibration 12 in CP, NP and AP, respectively, with PED 52%, 39% and 43%, from its own corresponding coordinate. It

mixes with several other normal modes in these molecules. The details can be found in Tables 2–4.

The vibrational modes, 6a and 6b were identified and assigned from careful consideration of their characteristic eigenvector distribution. The C–C–C angles change in the ratio +2, –1, –1, +2, –1, –1 in mode 6a, whereas they change in the ratio 0, +2, –2, 0, +2, –2 in mode 6b. Significant PED contribution comes from the corresponding  $\angle$ CCC bending modes to these vibrations. For instance, the IR band at  $580\text{ cm}^{-1}$  gets 42% PED from mode 6a, whereas the Raman shift around  $622\text{ cm}^{-1}$  has 65% PED from mode 6b, in CP. Bands that can be considered 6a and 6b in NP and AP can be read from Tables 3 and 4, respectively.

A characteristic feature of mode 1 is that all ring C–C bonds, either increase or decrease at the same time. In benzene this frequency is a pure C–C stretching fundamental as it is totally symmetric and occurs in a spectral region that is far away from C–H stretching region. As these restrictions are removed from the present set of molecules, mode 1 can mix with several bending modes and in particular with lower frequencies of substituent stretching vibrations. As a result, mode 1 cannot maintain its purity, in the present set molecules, as in benzene. Based on the present calculations, the bands near  $792\text{ C}$ ,  $1044$  and  $758\text{ cm}^{-1}$  are attributed to mode 1 in CP, NP and AP, respectively. Tables 2–4, reveal its mixing with other normal modes.

**4.2.1.4. C–H out-of-plane bending modes.** Another name for these vibrations is C–H wagging modes. They are labeled 5, 11 and 17b in the present set of molecules. There is no difficulty in identifying the bands around  $861\text{ R}$ ,  $919$  and  $839\text{ R cm}^{-1}$  with mode 5, in CP, NP and AP, respectively, as significant PED comes from the corresponding C–H wagging coordinate, which falls in the range 57 to 84%. In the same way, it is easy to ascribe the normal modes at  $758$ ,  $786\text{ C}$  and  $741\text{ C cm}^{-1}$  to fundamental 11, based on high PED contribution from related C–H wagging coordinate, which varies from 46 to 75%, in CP, NP and AP, respectively. Similarly, there is no problem in associating the fundamentals near  $834\text{ C}$ ,  $860$  and  $821\text{ cm}^{-1}$  with vibration 17b due to dominant PED drawn from relevant C–H wagging coordinate, which is in the range 33 to 49%, in CP, NP and AP, respectively. It is to be noted that the attribution of IR absorption in the vicinity of  $919$ ,  $786\text{ C}$  and  $860\text{ cm}^{-1}$  in NP to mode 5, 11 and 17b compare nicely with those of the corresponding bands in 2,5-dihydroxytoluene in the neighborhood of  $933$ ,  $819$  and  $878\text{ cm}^{-1}$ , respectively.<sup>49</sup>

**4.2.1.5. Ring torsions.** Normal modes 4, 16a and 16b are called the ring torsions in benzene and its derivatives. Vibration 4 is identified at  $694$ ,  $722\text{ C}$  and  $728\text{ R cm}^{-1}$  in CP, NP and AP, respectively. It essentially results from mixing of mode 4 with normal frequencies  $4'$ , 10a and 10b; 11, 10a and 10b; and 11, 10a,  $4'$  and 17b in CP, NP and AP, respectively. Vibration 16a is assigned to the Raman shifts near  $446$  and  $424\text{ cm}^{-1}$  in CP and NP, respectively, whereas it is located around  $428\text{ cm}^{-1}$  in IR absorption, in AP. Similarly, vibration 16b is ascribed to  $581\text{ C}$ ,  $500$  and  $600\text{ R cm}^{-1}$  in CP, NP and AP, respectively. Mixed nature of 16a and 16b can be understood from Tables 2–4.

**4.2.1.6. Vibrations associated with the bonds linking phenyl ring to the substituent groups.** These are inter-ring C–C bond, phenolic C–O bond, C–Cl bond and nitro and amino C–N bonds.

**4.2.1.6.1. Vibrations of the inter-ring C–C bond.** There are four vibrations associated with C–C inter-ring bond that are to be considered here. These are  $\nu(\text{C–C}7)13$ ,  $\beta(\text{C–C}7)15$ ,  $\pi(\text{C}7\text{–C})10\text{b}$  and  $\tau(\text{C–C}7)$ . As predicted by the present computations, the Raman shifts at  $712$ ,  $301$ ,  $74$  and scaled value near  $44\text{ cm}^{-1}$  are assigned to the inter-ring C–C bond stretching vibration 13, its associated in-plane bending mode 15, related wagging fundamental 10b and relevant torsion frequency in CP, respectively. In NP, the Raman shifts around  $740$ ,  $292$ ,  $70$ , along with scaled value at  $46\text{ cm}^{-1}$  are due to the vibrations 13, 15, 10b and torsion of inter-ring C–C bond, respectively.

Similarly in AP, the IR absorptions near 696, 298 C, 69 C and 54 C  $\text{cm}^{-1}$  are identified with normal modes 13, 15, 10b and  $\tau(\text{C}-\text{C}7)$ , respectively. However, it is important to bear in mind that the former three vibrations are a result of mixing of several fundamentals, whereas the last one is predominantly torsion mode of the inter-ring C-C bond. The details can be read from Tables 2–4. These assignments for modes 13, 15 and inter-ring torsion in the three molecules coincide to a good degree of accuracy with those of corresponding bands in biphenyl-2-carboxaldehyde at 731, 277 C and 45 C  $\text{cm}^{-1}$ , respectively.<sup>47</sup> Obviously, same degree of coincidence cannot be expected for the wagging mode, due to mass differences involved in the substituted phenyl ring part of the biphenyl ring.<sup>47</sup>

**4.2.1.6.2. Vibrations of the phenolic C–O bond.** These are  $\nu(\text{C}-\text{O})7\text{a}$ ,  $\beta(\text{C}-\text{O})9\text{b}$  and  $\pi(\text{C}-\text{O})10\text{a}$ , that are common to the three molecules CP, NP and AP. On the basis of present computations the fundamentals at 1225, 1247 and 1251  $\text{cm}^{-1}$ ; 411 R, 399 C and 562 C  $\text{cm}^{-1}$ ; and 380 C, 204 C and 325 C  $\text{cm}^{-1}$  are ascribed to modes 7a, 9b and 10a, respectively, in CP, NP and AP. As can be seen from Tables 2–4, these vibrations are mixed normal modes.

**4.2.1.6.3. Vibrations of the C–Cl bond.** Stretching, in-plane and out-of-plane bending vibrations having their origin in the C–Cl bond, in CP, are designated 7b, 9a and 17a, respectively. Raman shifts near 180 and 150  $\text{cm}^{-1}$  are identified with  $\beta(\text{C}-\text{Cl})9\text{a}$  and  $\pi(\text{C}-\text{Cl})17\text{a}$ , whereas that predicted at 224  $\text{cm}^{-1}$  is attributed to  $\nu(\text{C}-\text{Cl})7\text{b}$ . Mode 7b is C–Cl stretch to the extent of 65%, whereas vibration 9a exhibits 55% C–Cl in-plane bending nature.

**4.2.1.6.4. Vibrations of the nitro and amino (C–N) bonds.** C–N bond is present in both NP and AP, each being responsible for three vibrations associated with the C–N bond. The IR absorption at 1076  $\text{cm}^{-1}$  in NP is a mixed mode of vibrations 12, 19b, 7b, 19b' and 18b with PED 23%, 18%, 12%, 9% and 8%, respectively. Similarly, the IR band around 1194  $\text{cm}^{-1}$  in AP is also a mixed vibration of modes 7b, 18a, 7a, 12, 13 and  $\beta(\text{OH})$  having PED contribution 23%, 22%, 11%, 11%, 9% and 5%, respectively, in AP. We find that the stretching frequency of amino C–N bond near 1194  $\text{cm}^{-1}$  is higher than that of nitro C–N bond stretching around 1076  $\text{cm}^{-1}$ . This result is consistent with higher bond length of nitro C–N bond (1.453 Å); in comparison with that of amino C–N bond (1.394 Å). This is further supported by the lower value of nitro C–N stretching force constant, which is 5.080 mdyne  $\text{Å}^{-1}$ , in comparison with that for amino C–N bond at 6.119 mdyne  $\text{Å}^{-1}$ . These results are a consequence of deactivating nitro group in NP and activating amino group in AP, to certain extent only. Because the systematics shown by C–N stretching frequencies and associated force constants of NP and AP cannot be attributed entirely to the movement of electron charge alone, as they are known to depend, to a significant extent, on the effective mass of NP and AP in general, and that of nitro and amino moieties in particular. There is no difficulty in assigning Raman shift near 178  $\text{cm}^{-1}$ , with 61% PED from vibration 9a, and the scaled value at 143  $\text{cm}^{-1}$  with 45% PED from mode 17a, in NP, to the normal modes  $\beta(\text{C}-\text{N})9\text{a}$  and  $\pi(\text{C}-\text{N})17\text{a}$ , respectively. The scaled values around 291 and 218  $\text{cm}^{-1}$ , attributable to modes 9a and 17a, in AP, are in fact arise due to participation of several vibrations as evident from Table 4.

#### 4.2.1.7. Vibrations of the substituent groups.

**4.2.1.7.1. Vibrations of the nitro group.** These comprise of six vibrations  $\nu_{\text{as}}(\text{NO}_2)$ ,  $\nu_{\text{s}}(\text{NO}_2)$ ,  $\delta(\text{NO}_2)$ ,  $\omega(\text{NO}_2)$ ,  $\gamma(\text{NO}_2)$  and  $\tau(\text{NO}_2)$ , which are present in NP only. The absorptions near 1538, 1371, 822R, 639, 560 and 87 C  $\text{cm}^{-1}$  are attributed to the above vibrations in NP, respectively. It is to be noted that significant PED contribution, ranging from 32% to 57% comes from the corresponding mode of the nitro group except  $\nu_{\text{as}}(\text{NO}_2)$ . As these vibrations are situated in a complex region of vibrational space, they are expected to mix with several other frequencies that fall in the same region. This is, indeed, found true in Table 3. These assignments for asymmetric stretching,

symmetric stretching, in-plane deformation and rocking vibrations of the nitro group in NP, agree well with those of corresponding modes in monohalogenated nitrobenzenes,<sup>50</sup> in the vicinity of 1520, 1350, 860 and 540  $\text{cm}^{-1}$ . This is also true of scaled value for torsion mode of the nitro group at 87  $\text{cm}^{-1}$ , as it is close to corresponding observed mode near 80–90  $\text{cm}^{-1}$  in several monohalogenated nitrobenzenes.<sup>50</sup>

**4.2.1.7.2. Vibrations of the amino group.** These are relevant for AP only. The symmetric and asymmetric stretching vibrations of the amino group occur at 3373 and 3287  $\text{cm}^{-1}$  in the solid phase. Both of them are pure as PED contribution from their corresponding coordinates is 100%. In-plane deformation of the amino group is identified with infrared absorption near 1602  $\text{cm}^{-1}$ . This is almost a pure mode, as it gets 88% PED from its own coordinate, with a minor contribution (7%) from amino C–N stretching vibration. Rocking mode of the amino group is assigned to the Raman shift near 1101  $\text{cm}^{-1}$ , having 25% PED from its own coordinate and mixing with mode 14 (32%), in-plane bending of OH moiety (27%) and 18b (9%). Similarly, IR absorption in the neighborhood of 511  $\text{cm}^{-1}$  with 27% PED, and Raman shift in the vicinity of 344  $\text{cm}^{-1}$  with 47% PED, from wagging and torsion vibration of the amino group are ascribed to  $\omega(\text{NH}_2)$  and  $\tau(\text{NH}_2)$ , respectively. Obviously, they cannot be pure modes (see Table 4). The assignments for in-phase vibrations of the amino moiety  $\nu_{\text{as}}(\text{NH}_2)$ ,  $\nu_{\text{s}}(\text{NH}_2)$ ,  $\delta(\text{NH}_2)$  and  $\gamma(\text{NH}_2)$  agree reasonably well with those of the corresponding IR absorptions around 3395, 3204, 1600 and 1048  $\text{cm}^{-1}$ , in 2-((2-aminopyridin-3-yl) methylene) hydrazinecarbothioamide<sup>51</sup> and its N-ethyl variant at 3362, 3197, 1584 and 1028  $\text{cm}^{-1}$ ,<sup>52</sup> respectively, obtained with same level of theory as in the present case.

**4.2.1.7.3. Vibrations of the hydroxyl moiety.** The three vibrations  $\nu(\text{OH})$ ,  $\beta(\text{OH})$  and  $\tau(\text{OH})$  (the twist is around C–O bond of COH moiety, hence, it can also be designated  $\tau(\text{C–O})$ ) belong to this category. The IR absorptions at 3346, 3450 and 3469  $\text{cm}^{-1}$ , in CP, NP and AP, respectively, are pure and assignable to OH stretching vibrations, as the corresponding coordinate contributes 100% PED to them. Raman shift at 1158  $\text{cm}^{-1}$  in CP, along with IR absorptions near 1170 and 1106  $\text{cm}^{-1}$ , in NP and AP, respectively, are attributed to in-plane bending mode of the OH moiety. It gets 36%, 21% and 20% PED from its own coordinate in CP, NP and AP, respectively. There are several other vibrations that take part in this normal mode, as it appears in a complicated region of vibrational spectrum in these molecules (see Tables 2–4). The torsion vibration of OH group is identified with the bands around 370 R, 668 and 254 C in CP. NP and AP, wherein the PED from the corresponding coordinate varies from 63 to 86%. It shows considerable mixing with ring torsion 16a in NP, whereas in CP and AP, this vibration does not exhibit any such mixing with other vibrations. The assignments for  $\nu(\text{OH})$  and  $\beta(\text{OH})$  in CP, NP and AP are acceptable, when compared to the attribution of corresponding vibrations for one of the hydroxyl fragment in 2,6-dihydroxytoluene.<sup>49</sup>

Discussion of attribution of C–H stretching vibrations in detail is not required as all of them are pure having 94–100% PED from corresponding C–H stretching coordinate. Further, the assignment of vibrations originating from the non-phenolic ring of CP, NP and AP, can be understood with the help of PED in Tables 2–4.

### 4.3. NMR spectral analysis

The NMR serves as a great resource in determining the structure of an organic compound by revealing its hydrogen and carbon skeleton. In order to make a definite assignment and analysis of  $^{13}\text{C}$  and  $^1\text{H}$  NMR spectra, theoretical calculations on chemical shifts of CP, NP and AP are undertaken, as explained in Section 3 dealing with computational aspects. Chemical shifts measured for CP and NP, in a solution of  $\text{CDCl}_3$ , and those obtained for AP in a solution of  $\text{DMSO-d}_6$ , employing TMS as internal standard are depicted in Figure SF1 ( $^1\text{H}$  spectra) and Figure SF2 ( $^{13}\text{C}$  spectra) (see supplementary information).

**Table 5.** Experimental and calculated  $^1\text{H}$  and  $^{13}\text{C}$  NMR chemical shifts  $\delta$  (ppm) of CP, NP and AP.

Atom	CP		NP		AP	
	Experimental	Calculated	Experimental	Calculated	Experimental	Calculated
H13	7.635	7.707	7.842	7.732	7.496	7.705
H14	7.409	7.548	7.413	7.603	7.262	7.590
H15	7.427	7.565	7.580	7.646	7.226	7.559
H16	7.584	7.685	7.864	7.778	7.372	7.641
H17	7.390	7.533	7.489	7.629	7.399	7.653
H18	7.488	7.622	8.544	8.498	6.946	7.071
H21	7.166	7.281	7.267	7.438	6.751	6.899
H22	7.283	7.478	8.337	8.005	6.748	6.840
H23	5.734	5.309	10.607	11.353	9.234	9.125
H24	–	–	–	–	4.959	3.577
H25	–	–	–	–	4.959	3.929
RMSD	0.19		0.29		0.56	
C1	139.603	147.550	138.239	145.771	144.723	149.507
C2	127.202	132.467	126.695	132.262	126.582	132.285
C3	128.866	133.562	129.123	133.838	129.105	133.304
C4	120.375	131.594	127.992	132.582	126.125	130.808
C5	128.950	133.710	129.145	134.177	129.129	133.378
C6	126.785	131.890	126.689	132.076	126.350	132.070
C7	135.054	142.582	133.871	141.137	136.645	142.884
C8	127.342	132.714	122.812	128.914	115.226	117.816
C9	126.760	131.887	133.792	140.218	132.106	140.676
C10	150.801	157.160	154.356	162.872	141.487	148.418
C11	116.626	120.375	120.425	124.681	113.500	117.388
C12	127.588	132.923	136.278	144.358	115.854	120.419
RMSD	6.34		6.28		5.39	

–: Not relevant.

Observed and calculated chemical shifts are summarized in Table 5 for both  $^1\text{H}$  and  $^{13}\text{C}$  NMR signals. The RMSD value for  $^1\text{H}$  NMR, between the experimental and computed chemical shifts is 0.19, 0.29 and 0.56 ppm, whereas the same quantity for  $^{13}\text{C}$  NMR is 6.34, 6.28 and 5.39 ppm, for CP, NP and AP, respectively. These are acceptable, as they are small. The linear regression between the experimental and calculated chemical shifts obtained by DFT method for  $^1\text{H}$  and  $^{13}\text{C}$  are plotted in Figure FS3 and Figure FS4, for CP, NP and AP, respectively. The correlation coefficients for proton chemical shifts are 0.990, 0.955 and 0.989, whereas those for carbon-13 chemical shifts are 0.945, 0.982 and 0.984, respectively, for CP, NP and AP. As these are close to unity the assignments made for NMR signals are reliable.

The chemical shifts, both experimental and theoretical, for the  $^1\text{H}$  atoms on the biphenyl ring appear in the range 6.748–8.544 ppm in the titled molecules. They are assigned for five hydrogen atoms on the phenyl ring, attached to the phenolic ring below.

CP:  $^1\text{H}$  NMR ( $\text{CDCl}_3$ , 400 MHz):  $\delta$  (ppm) = 7.64 (d,  $J$  = 2.1 Hz, 1H), 7.61–7.46 (m, 5H), 7.40 (dd,  $J$  = 13.5, 6.2 Hz, 1H), 7.17 (d,  $J$  = 8.4 Hz, 1H) and 5.73 (s, 1H, –OH).

NP:  $^1\text{H}$  NMR ( $\text{CDCl}_3$ , 400 MHz):  $\delta$  (ppm) = 10.61 (s, 1H, –OH), 8.34 (d,  $J$  = 2.3 Hz, 1H), 7.85 (dd,  $J$  = 8.7, 2.3 Hz, 1H), 7.60–7.39 (m, 5H) and 7.28 (d,  $J$  = 4.40 Hz, 1H).

AP:  $^1\text{H}$  NMR ( $\text{DMSO}-d_6$ , 400 MHz):  $\delta$  (ppm) = 9.23 (s, 1H, –OH), 7.52–7.22 (m, 5H), 6.95 (d,  $J$  = 2.34 Hz, 1H), 6.76 (dd,  $J$  = 0.96, 5.77 Hz, 1H), 6.74 (d,  $J$  = 4.20 Hz, 1H), and 4.96 (s, 2H, –NH<sub>2</sub>).

The  $^{13}\text{C}$  NMR chemical shifts for an organic compound are usually greater than 100 ppm.<sup>53,54</sup> In the present investigation also,  $^{13}\text{C}$  NMR chemical shifts are greater than 100 ppm. They vary from 117.388 to 162.872 ppm for carbons, as per present calculations for CP, NP and AP. The variation of chemical shifts depends on the decrease in electron donating or shielding ability of the attached atoms.<sup>55</sup> The molecules CP, NP and AP consist of twelve carbon atoms each, and all of them are aromatic carbons associated with biphenyl unit shown in Figure 1. As expected we find twelve  $^{13}\text{C}$  chemical shifts in NMR spectra of CP, NP and AP, each.

They are assigned below.

CP:  $^{13}\text{C}$  NMR ( $\text{CDCl}_3$ , 400 MHz):  $\delta$  (ppm) = 150.801, 139.603, 135.054, 128.950, 128.866, 127.588, 127.342, 127.202, 126.785, 126.760, 120.375 and 116.626.

NP:  $^{13}\text{C}$  NMR ( $\text{CDCl}_3$ , 400 MHz):  $\delta$  (ppm) = 154.356, 138.239, 136.278, 133.871, 133.792, 129.145, 129.123, 127.992, 126.695, 126.689, 122.812 and 120.425.

AP:  $^{13}\text{C}$  NMR ( $\text{DMSO-d}_6$ , 400 MHz):  $\delta$  (ppm) = 144.723, 141.487, 136.645, 132.106, 129.129, 129.105, 126.582, 126.350, 126.125, 115.854, 115.226 and 113.500.

#### 4.4. Frontier molecular orbitals

Frontier molecular orbitals facilitate proper understanding of the electronic transitions. They have significant role in quantum chemistry for determining the molecular reactivity of conjugated systems<sup>56</sup> and capability of a molecule to absorb electromagnetic radiation. HOMO plays the role of an electron donor, whereas LUMO acts as the electron acceptor.<sup>36,37</sup>

##### 4.4.1. Analysis of UV-Vis spectra

The electronic absorption spectra of CP, NP and AP were computed with the help of calculations using TD-DFT/B3LYP/6-311++G(d,p) method using the Polarizable Continuum Model (PCM) through the integrated equation formalism (IEF-PCM), to take care of solvent effects,<sup>35</sup> as already mentioned in Section 3. The observed and simulated UV-Vis spectra of the molecules CP, NP and AP are shown in Figure FS5, and corresponding spectral values are presented in Table ST1 (see supplementary information).

The experimental UV-Vis spectra, in solution, show two absorption bands ( $\lambda_{\text{max}}$ ) at 305 and 250 nm in CP; 455 and 306 nm in NP; and 305 and 260 nm in AP. In simulated UV-Vis spectra the absorption bands at 271.60, 264.24 and 255.95 nm for CP; 436.55, 343.79 and 315.01 nm for NP; and 301.16, 278.71 and 268.75 nm for AP, with associated oscillator strengths  $f=0.2751$ , 0.3419 and 0.0041 for CP; 0.0495, 0.0002 and 0.0150 for NP; and 0.2122, 0.0012 and 0.0481 for AP, respectively, are predicated as in Table ST1. Calculations show that the higher of the two observed absorptions is a  $n\rightarrow\pi^*$  transition, whereas the lower one is a  $\pi\rightarrow\pi^*$  transition. Further, the major contribution of molecular orbitals for the maximum absorption wavelength corresponds to the electronic transition from the H $\rightarrow$ L (57%) and H-1 $\rightarrow$ L+1 (34%) for CP; H $\rightarrow$ L (98%) for NP; and H $\rightarrow$ L (92%) for AP. The other remaining electronic transitions are available in Table ST1. These transitions, along with their corresponding energy gaps are shown in Figure 8.

##### 4.4.2. Chemical reactivity descriptors

Frontier molecular orbitals (HOMO and LUMO) and their properties, such as energies, play a vital role in chemical reactions. The frontier orbital energy gap between HOMO and LUMO helps to characterize the chemical reactivity, kinetic stability and polarizability of a molecule.<sup>57</sup> A small HOMO-LUMO energy gap implies low kinetic stability and high chemical reactivity since it is energetically favorable to accumulate electrons in high-lying LUMO by exciting electrons from low-lying HOMO.<sup>58-61</sup> Large energy gap between two frontier orbitals is a reflection of greater hardness of the molecule. Chemical hardness is a useful concept for understanding the behavior of chemical systems. It is known that soft molecules have small energy gap and hence are more polarizable making them chemically more reactive than hard molecules.<sup>62</sup> The electrophilicity index is an indicator of electron flow between a donor and an acceptor.<sup>63</sup>

The energies of HOMO-LUMO orbitals, and various indicative parameters of chemical reactivity, obtained as a result of computations at B3LYP/6-311++G(d,p) level for CP, NP and AP are presented in Table ST2 (see Figure 8 also). It is seen from Table ST2, the difference between the



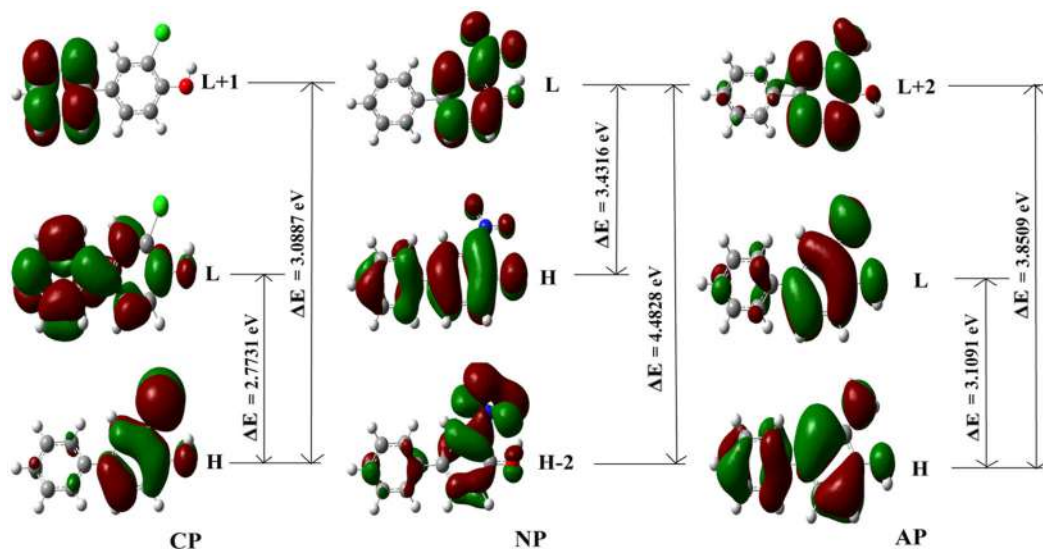


**Figure 8.** Frontier molecular orbitals of CP, NP and AP.

HOMO and LUMO orbital energies is 2.7731, 3.4316 and 3.1091 eV in CP, NP and AP, respectively. The values of chemical hardness and softness are 1.3865 and 0.3606 eV for CP; 1.7158 and 0.2914 eV for NP; and 1.5545 and 0.3216 eV for AP, respectively. It can also be seen from [Table ST2](#) (depicted as [supplementary information](#)), the value of electrophilicity power ( $\omega$ ) of the three molecules is larger which indicates that these molecules are strong electrophilic due to small value of chemical potential.<sup>64</sup> The electrophilicity power of a given molecule can also be used to study the biological activity and toxicity of that molecule.<sup>65,66</sup>

#### 4.5. Non-linear optical (NLO) characteristics

Organic NLO materials are being investigated widely by means of DFT,<sup>67–70</sup> due to their potential applications for optical logic, optical switching, optical memory and frequency shifting.<sup>71–74</sup>

The values of total molecular dipole moment ( $\mu_t$ ) and its components, total molecular polarizability ( $\alpha_t$ ) and its components; and first order hyperpolarizability ( $\beta_t$ ) and its components of CP, NP and AP are computed with DFT employing B3LYP/6-311++G(d,p) level of theory using Gaussian 09 program. The results are summarized in [Table ST3](#) (see [supplementary information](#)).

The NLO behavior of a molecular system is usually evaluated by comparing its total molecular dipole moment ( $\mu_t$ ) and the mean first order hyperpolarizability ( $\beta_t$ ) with corresponding parameters of a prototypical molecule like Urea. Since, Urea is often considered to be a standard NLO material due to the combination of non-centrosymmetric crystal packing and capacity for intramolecular charge transfer. It is one of the standards among second-order NLO materials which demonstrate the electrooptic effect by which an external field changes the refractive index and second harmonic generation (SHG), where the material scatters the light at twice the frequency of the incident light. The efficiency of both NLO processes is determined by the second-order susceptibility, which vanishes in centrosymmetric media. Therefore, the possibility to design photonic devices at smaller scale critically depends on new non-centrosymmetric materials with high nonlinear susceptibility.<sup>75</sup> Moreover, Urea does not exhibit a large nonlinearity compared to visible absorbing molecules. Its second order nonlinearity is substantially larger than that of other organic molecules, such as fluorobenzene, aniline, nitrobenzene, p-nitroaniline and merocyanine



with comparable UV transparency.<sup>76</sup> Hence, Urea is considered as standard molecule to study the NLO behavior of a molecule.

The values of  $\mu_t$  and  $\beta_t$  for Urea are 1.3732 Debye and  $372.8 \times 10^{-33} \text{ cm}^5/\text{esu}$ , respectively, which are used frequently as threshold values.  $\mu_t$  is estimated at 0.4306, 1.6847 and 0.5590 Debye, respectively, for CP, NP and AP, whereas  $\beta_t$  for them is predicted near  $876.7213 \times 10^{-33}$ ;  $562.4747 \times 10^{-33}$  and  $1247.6376 \times 10^{-33} \text{ cm}^5/\text{esu}$ . Thus, we find that the value of  $\mu_t$  for NP is higher, and those for CP and AP are lower than the threshold value of Urea, whereas value of  $\beta_t$  for CP, NP and AP is 2.35, 1.51 and 3.35 times higher than the threshold value of Urea. Hence, due to this relatively higher value of hyperpolarizability for CP, NP and AP, with respect to corresponding parameter for Urea, they are potential candidates for NLO applications. Hyperpolarizability of a molecule is caused by movement of electron cloud through  $\pi$ -conjugated structure of electrons.<sup>77</sup> The charge delocalization in the molecule can be understood from the components of hyperpolarizability. The maximum charge delocalization occurs along  $\beta_{xxx}$  in the molecules CP and AP, and  $\beta_{xxy}$  in NP, as evidenced from Table ST3 (see supplementary information).

#### 4.6. Thermodynamic parameters and rotational constants

Various calculated thermodynamic parameters and rotational constants for CP, NP and AP are collected in Table ST4 (see supplementary information). The standard thermodynamic functions such as SCF energy, specific heat capacity at constant volume ( $C_v$ ), entropy (S), vibrational energy ( $E_{\text{vib}}$ ), zero-point energy ( $E_0$ ) and rotational constants (A, B and C) are evaluated employing rigid rotor harmonic oscillator approximation employing standard expressions,<sup>78–80</sup> using DFT/B3LYP/6-311++G(d,p) level of theory. The rotational constants A, B and C are calculated at 1499, 306 and 262 MHz for CP; 1259, 283 and 237 MHz for NP; and 1999, 351 and 309 MHz for AP, respectively. Calculation of thermodynamic parameters is performed in gas phase and pertains to one mole of ideal gas at one atm pressure. As per the second law of thermodynamics in thermochemical field,<sup>81</sup> the results of present calculations can be used to compute the other thermodynamic energies and help to estimate the direction of chemical reactions.

#### 4.7. Natural bond orbital (NBO) analysis

The NBO analysis provides a description of the structure of a conformer by a set of localized bond and antibond orbitals; and Rydberg extra valence orbitals. It tells about the interaction between the bond orbitals, electron delocalization, bond bending effect, intra-molecular charge transfer (ICT) and identification of hydrogen bonding.<sup>82</sup> In the NBO analysis,<sup>40,83,84</sup> the electron wave functions are interpreted in terms of a set of occupied Lewis-type (bond or lone pair) and a set of unoccupied non-Lewis-type (anti-bond or Rydberg) localized NBO orbitals. The delocalization of electron density (ED) among these orbitals causes a stabilizing donor-acceptor interaction. The stabilization energies of all possible interactions between donor and acceptor orbitals in the NBO basis can be evaluated using the second order perturbation theory. The interaction yields in a loss of occupancy from the localized NBO of the idealized Lewis structure into an empty non-Lewis orbital. The delocalization effects (or donor-acceptor charge transfers) can be estimated from the off-diagonal elements of the Fock matrix in the NBO basis. So, the natural bond orbital (NBO) computations are made using NBO 3.1 program<sup>85</sup> as implemented in the Gaussian 09 W software at the DFT/B3LYP level using 6-311++G(d,p) basis set, in order to understand various second-order interactions between the filled orbitals of one subsystem and vacant orbitals of another subsystem. The output obtained by second-order perturbation theory is used for identifying the significant delocalization effects. The strength of these delocalization interactions  $E(2)$  is evaluated by the method reported by A. E. Reed et al.<sup>40</sup>

The larger the  $E(2)$  value, the stronger is the interaction between electron donors and acceptors, i.e. the more electron donating tendency from electron donors to acceptors and greater the extent of conjugation of the whole system. The dominant contributors, to the stabilization energies, that emerge from NBO analysis for CP, NP and AP are presented in Tables ST5, ST6 and ST7, respectively. The molecular interaction is formed by the orbital overlap between  $\sigma(\text{C-C})$  and  $\sigma^*(\text{C-C})$  bond orbitals, which results in intra-molecular charge transfer (ICT) causing stabilization of the molecule. Large value of interaction energy indicates weakening of the corresponding bonds. The intra-molecular hyper conjugative energy between  $\sigma$  and  $\sigma^*$  electrons of aromatic ring is found at  $4.88 \text{ kcal mol}^{-1}$  due to interactions  $\sigma(\text{C10-C11}) \rightarrow \sigma^*(\text{C9-C10})$  in CP, whereas  $4.54 \text{ kcal mol}^{-1}$  for the interaction of  $\sigma(\text{C9-C10}) \rightarrow \sigma^*(\text{C8-C9})$  in NP; while it is  $4.56 \text{ kcal mol}^{-1}$  for the interaction of  $\sigma(\text{C10-C11}) \rightarrow \sigma^*(\text{C9-C10})$  in AP.

The electron density at the conjugated  $\pi$ -bonds of the biphenyl unit is in the range 1.6405–1.7007, 1.6150–1.7044 and 1.6369–1.7030 in CP, NP and AP, respectively, whereas that for  $\pi^*$ -antibonds are in the range between 0.3234–0.4481, 0.3057–0.4525 and 0.3258–0.3960.

According to NBO analysis, the interactions  $\pi(\text{C1-C6}) \rightarrow \pi^*(\text{C4-C5})$ ;  $\pi(\text{C2-C3}) \rightarrow \pi^*(\text{C1-C6})$ ;  $\pi(\text{C4-C5}) \rightarrow \pi^*(\text{C2-C3})$ ;  $\pi(\text{C7-C8}) \rightarrow \pi^*(\text{C11-C12})$ ;  $\pi(\text{C9-C10}) \rightarrow \pi^*(\text{C7-C8})$ ;  $\pi(\text{C11-C12}) \rightarrow \pi^*(\text{C9-C10})$  and  $\text{LP}(2)\text{O20} \rightarrow \pi^*(\text{C9-C10})$  have high stabilization energy in the range  $20.56\text{--}31.15 \text{ kcal mol}^{-1}$ , respectively, in CP; the interactions  $\pi(\text{C1-C2}) \rightarrow \pi^*(\text{C3-C4})$ ;  $\pi(\text{C3-C4}) \rightarrow \pi^*(\text{C1-C2, C5-C6})$ ;  $\pi(\text{C5-C6}) \rightarrow \pi^*(\text{C1-C2, C3-C4})$ ;  $\pi(\text{C7-C8}) \rightarrow \pi^*(\text{C11-C12})$ ;  $\pi(\text{C9-C10}) \rightarrow \pi^*(\text{C7-C8, N19-O24})$ ;  $\pi(\text{C11-C12}) \rightarrow \pi^*(\text{C9-C10})$ ,  $\text{LP}(2)\text{O20} \rightarrow \pi^*(\text{C9-C10})$  and  $\text{LP}(3)\text{O25} \rightarrow \pi^*(\text{N19-O24})$  have high stabilization energy in the range  $20.03\text{--}126.90 \text{ kcal mol}^{-1}$ , respectively in NP; and  $\pi(\text{C1-C6}) \rightarrow \pi^*(\text{C4-C5})$ ;  $\pi(\text{C2-C3}) \rightarrow \pi^*(\text{C1-C6})$ ;  $\pi(\text{C4-C5}) \rightarrow \pi^*(\text{C2-C3})$ ;  $\pi(\text{C7-C12}) \rightarrow \pi^*(\text{C10-C11})$ ;  $\pi(\text{C8-C9}) \rightarrow \pi^*(\text{C7-C12})$  and  $\text{LP}(2)\text{O20} \rightarrow \pi^*(\text{C10-C11})$  interactions have high stabilization energy in the range  $20.48\text{--}24.09 \text{ kcal mol}^{-1}$ , respectively, in AP. Due to movement of  $\pi$ -electron cloud from donor to acceptor (i.e. ICT), the molecules get more polarized. This leads us to the inference that the NLO properties of CP, NP and AP arise from ICT. This result is in supports of our earlier observation that the three materials are good for nonlinear applications, made in the section on NLO properties. As a consequence of this charge delocalization, the molecule gains total stabilization energy  $258.03$ ,  $254.67$  and  $254.81 \text{ kcal mol}^{-1}$  in CP, NP and AP, respectively from the biphenyl unit alone. The stabilization energies due to charge transfer from lone pairs of oxygen, nitrogen and chlorine atoms to various other bonds that weaken and elongate the bonds in the three molecules under investigation can be found in Tables ST5–ST7.

#### 4.8. Analysis of molecular electrostatic surface potential (MESP)

The molecular electrostatic surface potential (MESP) is the net electrostatic effect of a molecule in the surrounding space and is well defined by the total charge distribution (nuclei and electrons). The MESP correlates with the partial charges, dipole moment, electronegativity and chemical reactivity of a given molecule,<sup>86–88</sup> non-covalent interactions, particularly, hydrogen bonds<sup>89–91</sup> and molecular aggregation,<sup>92,93</sup> lone pair- $\pi$  interactions,<sup>94,95</sup> aromaticity and reaction mechanisms.<sup>96,97</sup> Molecular electrostatic surface potential has been plotted for CP, NP and AP molecules with DFT/B3LYP/6-311++G(d,p) formalism. The negative (electron rich) regions, represented by red color, in the MESP diagram are related to electrophilic reactivity while the positive (electron deficient) regions, represented by the blue region, are related to nucleophilic reactivity. MESP plots are shown, in Figure SF6, for the molecules under investigation. It can be seen from this figure that the maximum negative electrostatic potential region is located over the oxygen atoms, which are prone to the electrophilic reactions, whereas regions having the positive electrostatic potential are around the hydrogen atoms, which are preferentially nucleophilic reaction sites, in the three molecules under investigation.

## 5. Conclusions

Geometry optimization of structures revealed that the three molecules investigated are stabilized in the ground state with lowest energy in a non-planar structure belonging to  $C_1$  point group symmetry, forming intra-molecular hydrogen bond in three molecules. Conformational studies demonstrated that the hydrogen atom of hydroxyl moiety assumes *cis* position with respect to chlorine atom in CP, and nitrogen atom of nitro group in NP, whereas it prefers *trans* position with respect to nitrogen atom of amino group in AP. The steric repulsion of nitrogen atom of amino group in AP influences the C–N bond to be twisted since this group is more compact and light, whereas, chlorine atom and nitrogen atom, respectively in CP and NP retains in the same plane of phenolic ring due to their heavy mass. Evaluated geometry parameters obtained in DFT computations show good agreement with available experimental data. Proposed vibrational assignments exhibit reasonably good accordance with those of corresponding bands in related molecules. Deactivating nature of the nitro group in NP and activating property of amino moiety in AP are well manifested in C–N bond lengths at 1.453 Å and 1.394 Å, respectively. This result is substantiated by lower values of nitro C–N bond stretching frequency near  $1076\text{ cm}^{-1}$  and its associated C–N stretching force constant at  $5.080\text{ mdyne Å}^{-1}$ , in comparison with those of corresponding parameters around  $1194\text{ cm}^{-1}$  and  $6.119\text{ mdyne Å}^{-1}$  for amino C–N bond. Measured  $^1\text{H}$  and  $^{13}\text{C}$  NMR chemical shifts and electronic spectra concur satisfactorily with their simulated counterparts for the three molecules. FMO investigations showed that the studied molecules are highly reactive as the energy gap for them was comparatively small, and helped in the assignment of observed UV-Vis spectral bands. It was concluded on the basis of computed NLO parameters that CP, NP and AP were potentially good for NLO applications. It was found using NBO studies that intra-molecular charge transfer (ICT) imparts NLO properties to these molecules. The evaluated molecular electrostatic potentials proved that the most reactive site is in the vicinity of oxygen atoms in the three molecules investigated here.

## Acknowledgements

The authors sincerely acknowledge to Central Analytical Laboratory (CAL), BITS Pilani, Hyderabad, India (IR, NMR and UV-Vis) and Sophisticated Analytical Instruments Facility (SAIF) IIT-Madras, India for measurement of Raman spectra. The second author (KSS) is grateful to the management of SR University Warangal, India, for permitting him to undertake the reported investigations.

## Disclosure statement

No potential conflict of interest was reported by the author(s).

## ORCID

B. Venkatram Reddy  <http://orcid.org/0000-0001-6516-7731>

## References

1. Hong-Ming Cheng, Morifusa Eto, Shozo Kuwatsuka, and Yasuyoshi Oshima, "Studies on the Phenylphenol Derivatives with Biological Activity. Part I. Herbicidal Activity of Nitro-Substituted Phenylphenols," *Agricultural and Biological Chemistry* 32, no. 3 (1968): 345–52. doi:10.1080/00021369.1968.10859062
2. Hong-Ming Cheng, Morifusa Eto, Shozo Kuwatsuka, and Yasuyoshi Oshima, "Studies on the Phenylphenol Derivatives with Biological Activity. Part II. The Herbicidal Activity of Chloro-Substituted Phenylphenols," *Agricultural and Biological Chemistry* 32, no. 3 (1968): 353–8. doi:10.1080/00021369.1968.10859062
3. Hong-Ming Cheng, Morifusa Eto, Kanji Nakamura, Shozo Kuwatsuka, Yasuyoshi Oshima, and Masaru Kado, "Studies on the Phenylphenol Derivatives with Biological Activity. Part III. Fungistatic Activity of

- Phenylphenol Derivatives,” *Agricultural and Biological Chemistry* 32, no. 9 (1968): 1162–74. doi:10.1080/00021369.1968.10859205
4. Hong-Ming Cheng, Morifusa Eto, Eiji Taniguchi, Shozo Kuwatsuka, Yasuyoshi Oshima, and Masaru Kado, “Studies on Phenylphenol Derivatives with Biological Activity. Part V. Miticidal Activity and Effect on Oxidative Phosphorylation,” *Botyu-Kagaku* 34, no. 176 (1969): 176–82.
  5. Cora May Segura Savoy, and John Leo Abernethy, “The Halogenation of Certain Esters in the Biphenyl Series. II. The Chlorination of 4-Phenylphenyl Benzoate and 4-Phenylphenyl Benzenesulfonate,” *Journal of the American Chemical Society* 64, no. 9 (1942): 2219–21. doi:10.1021/ja01263a057
  6. Cora May Segura Savoy, and John Leo Abernethy, “The Halogenation of Certain Esters in the Biphenyl Series. I. The Chlorination of 4-Phenylphenyl Acetate,” *Journal of the American Chemical Society* 64, no. 11 (1942): 2719–20. doi:10.1021/ja01261a052
  7. Cora May Segura Savoy, and John Leo Abernethy, “Studies in the Biphenyl Series. III. The Attempted Chlorination of the Acetate, Benzoate and Benzenesulfonate of 4-(4-Chlorophenyl)-Phenol: 2-Chloro-4-(4-Chlorophenyl)-Phenol,” *Journal of the American Chemical Society* 65, no. 8 (1943): 1464–5. doi:10.1021/ja01248a007
  8. R. M. Holzem, H. M. Stapleton, and C. K. Gunsch, “Determining the Ecological Impacts of Organic Contaminants in Biosolids Using a High-Throughput Colorimetric Denitrification Assay: A Case Study with Antimicrobial Agents,” *Environmental Science & Technology* 48, no. 3 (2014): 1646–55. doi:10.1021/es404431k
  9. Carolyn Pratt Brock, and Kurt L. Haller, “Two Crystal Modifications of 4-Hydroxybiphenyl: The Biphenyl Structure without an Inversion Center and a Fully Ordered Structure Containing Nearly Planar Molecules,” *The Journal of Physical Chemistry* 88, no. 16 (1984): 3570–4. doi:10.1021/j150660a039
  10. Kihwan Bae, Sunghyen Koo, and Wonjun Seo, “Antimicrobial Activities of Hydroxybiphenyl Derivatives,” *Korean Journal of Pharmacognosy* 17, no. 1 (1986): 85–90.
  11. Wonjun Seo, Sunghyen Koo, and Kihwan Bae, “Antimicrobial Activities of Hydroxybiphenyl Derivatives (II). Synthesis and Antibacterial Activities of Allylhydroxybiphenyl Compounds against a Cariogenic Bacterium *Streptococcus mutans* ATCC OMZ176,” *Archives of Pharmacol Research* 9, no. 3 (1986): 127–30. doi:10.1007/BF02899995
  12. Nikola Basarić, Nikola Cindro, Damir Bobinac, Kata Mlinarić-Majerski, Lidija Uzelac, Marijeta Kralj, and Peter Wan, “Sterically Congested Quinone Methides in Photodehydration Reactions of 4-Hydroxybiphenyl Derivatives and Investigation of Their Antiproliferative Activity,” *Photochemical & Photobiological Sciences* 10, no. 12 (2011): 1910–25. doi:10.1039/c1pp05182b
  13. Edwin J. Routledge, and John P. Sumpter, “Structural Features of Alkylphenolic Chemicals Associated with Estrogenic Activity,” *The Journal of Biological Chemistry* 272, no. 6 (1997): 3280–8. doi:10.1074/jbc.272.6.3280
  14. A. H. Filbey, Jr. H. G. Braxton, and B. R. Meltsner, “Process for Preparing Benzyl Substituted Phenols, Dibenzyl Phenolic Compounds, and the Antioxidant Use of Such Phenols” (European Patent 0186255, filed February 28 1985, and issued July 02, 1986).
  15. G. Powis, D. C. Melder, and T. J. Wilke, “Human and Dog, but Not Rat, Isolated Hepatocytes Have Decreased Foreign Compound-Metabolizing Activity Compared to Liver Slices,” *Drug Metabolism and Disposition* 17, no. 5 (1989): 526–31.
  16. G. Powis, D. J. Moore, T. J. Wilke, and K. S. Santone, “A High-Performance Liquid Chromatography Assay for Measuring Integrated Biphenyl Metabolism by Intact Cells: Its Use with Rat Liver and Human Liver and Kidney,” *Analytical Biochemistry* 167, no. 1 (1987): 191–8. doi:10.1016/0003-2697(87)90151-5
  17. J. H. Burckhalter, F. H. Tendick, E. M. Jones, P. A. Jones, W. F. Holcomb, and A. L. Rawlins, “Aminoalkylphenols as Antimalarials. II. (Heterocyclic-Amino)- $\alpha$ -Amino-o-Cresols. The Synthesis of Camoquin,” *Journal of the American Chemical Society* 70, no. 4 (1948): 1363–73. doi:10.1021/ja01184a023
  18. María V. Castillo, Roxana A. Rudyk, Lilian Davies, and Silvia Antonia Brandán, “Analysis of the Structure and the FT-IR and Raman Spectra of 2-(4-Nitrophenyl)-4H-3,1-Benzoxazin-4-One. Comparisons with the Chlorinated and Methylated Derivatives,” *Journal of Molecular Structure* 1140 (2017): 2–11. doi:10.1016/j.molstruc.2016.08.070
  19. Axel D. Becke, “Density-Functional Thermochemistry. III. The Role of Exact Exchange,” *The Journal of Chemical Physics* 98, no. 7 (1993): 5648–52. doi:10.1063/1.464913
  20. C. Lee, W. Yang, and R. G. Parr, “Development of the Colle-Salvetti Correlation-Energy Formula into a Functional of the Electron Density,” *Physical Review. B, Condensed Matter* 37, no. 2 (1988): 785–9. doi:10.1103/physrevb.37.785
  21. M. J. Frisch, et al, *Gaussian 09, Revision B.01* (Wallingford, CT: Gaussian, Inc., 2010).
  22. R. Dennington, T. Keith, and J. Millam, *Gauss View, Version 5.0. 9* (Shawnee Mission: Semichem Inc., 2009).

23. Arne Almenningen, Otto Bastiansen, Liv Fernholt, Bjørg N. Cyvin, Sven J. Cyvin, and Svein Samdal, "Structure and Barrier of Internal Rotation of Biphenyl Derivatives in the Gaseous State," *Journal of Molecular Structure* 128, no. 1–3 (1985): 59–76. doi:[10.1016/0022-2860\(85\)85041-9](https://doi.org/10.1016/0022-2860(85)85041-9)
24. Xuqiang Chao, Xiuqin Zhang, Kai Wang, and Jun Ji, Qiang Chen, "4-Methoxy-3-Nitrobiphenyl," *Acta Crystallographica. Section E, Structure Reports Online* 68, no. Pt 1 (2012): o114. doi:[10.1107/S1600536811052846](https://doi.org/10.1107/S1600536811052846)
25. Hui-Fen Qian, and Wei Huang, "Biphenyl-3,3',4,4'-Tetraamine," *Acta Crystallographica. Section E, Structure Reports Online* 66, no. Pt 5 (2010): o1060. doi:[10.1107/S1600536810012511](https://doi.org/10.1107/S1600536810012511)
26. T. Sundius, "Molvib – A Flexible Program for Force Field Calculations," *Journal of Molecular Structure* 218 (1990): 321–6. doi:[10.1016/0022-2860\(90\)80287-T](https://doi.org/10.1016/0022-2860(90)80287-T)
27. T. Sundius, "Scaling of ab Initio Force Fields by MOLVIB," *Vibrational Spectroscopy* 29, no. 1–2 (2002): 89–95. doi:[10.1016/S0924-2031\(01\)00189-8](https://doi.org/10.1016/S0924-2031(01)00189-8)
28. Geza Fogarasi, Xuefeng Zhou, Patterson W. Taylor, and Peter Pulay, "The Calculation of ab Initio Molecular Geometries: efficient Optimization by Natural Internal Coordinates and Empirical Correction by Offset Forces," *Journal of the American Chemical Society* 114, no. 21 (1992): 8191–201. doi:[10.1021/ja00047a032](https://doi.org/10.1021/ja00047a032)
29. Peter Pulay, Geza Fogarasi, Gabor Pongor, James E. Boggs, and Anna Vargh, "Combination of Theoretical ab Initio and Experimental Information to Obtain Reliable Harmonic Force Constants. Scaled Quantum Mechanical (QM) Force Fields for Glyoxal, Acrolein, Butadiene, Formaldehyde, and Ethylene," *Journal of the American Chemical Society* 105, no. 24 (1983): 7037–47. doi:[10.1021/ja00362a005](https://doi.org/10.1021/ja00362a005)
30. J. F. Arenas, I. López Tocón, J. C. Otero, and J. I. Marcos, "Vibrational Spectra of Methylpyridines," *Journal of Molecular Structure* 476, no. 1–3 (1999): 139–50. doi:[10.1016/S0022-2860\(98\)00541-9](https://doi.org/10.1016/S0022-2860(98)00541-9)
31. Z. Latajka, W. B. Person, and K. Morokuma, "An Ab Initio Calculation of the Infrared Spectrum and Tautomerism of Guanine," *Journal of Molecular Structure: THEOCHEM* 135 (1986): 253–66. doi:[10.1016/0166-1280\(86\)80063-X](https://doi.org/10.1016/0166-1280(86)80063-X)
32. G. Keresztury, S. Holly, G. Besenyei, J. Varga, Aiyng Wang, and J. R. Durig, "Vibrational Spectra of Monothiocarbamates-II. IR and Raman Spectra, Vibrational Assignment, Conformational Analysis and Ab Initio Calculations of S-methyl-N,N-Diethyldithiocarbamate," *Spectrochimica Acta Part A: Molecular Spectroscopy* 49, no. 13–14 (1993): 2007–26. doi:[10.1016/S0584-8539\(09\)91012-1](https://doi.org/10.1016/S0584-8539(09)91012-1)
33. Gábor Keresztury, "Raman Spectroscopy: Theory," in *Hand Book of Vibrational Spectroscopy*, edited by John M. Chalmers and Peter R. Griffiths (New York: John Wiley and Sons Ltd., 2006), 71–87.
34. Krzysztof Wolinski, Robert Haacke, James F. Hinton, and Peter Pulay, "Methods for Parallel Computation of SCF NMR Chemical Shifts by GIAO Method: Efficient Integral Calculation, multi-Fock Algorithm, and Pseudodiagonalization," *Journal of Computational Chemistry* 18, no. 6 (1997): 816–25. doi:[10.1002/\(SICI\)1096-987X\(19970430\)18:6<816::AID-JCC7>3.0.CO;2-V](https://doi.org/10.1002/(SICI)1096-987X(19970430)18:6<816::AID-JCC7>3.0.CO;2-V)
35. Giovanni Scalmani, and Michael J. Frisch, "Continuous Surface Charge Polarizable Continuum Models of Solvation. I. General Formalism," *The Journal of Chemical Physics* 132, no. 11 (2010): 114110. doi:[10.1063/1.3359469](https://doi.org/10.1063/1.3359469)
36. Kenichi Fukui, "Role of Frontier Orbitals in Chemical Reactions," *Science* 218, no. 4574 (1982): 747–54. doi:[10.1126/science.218.4574.747](https://doi.org/10.1126/science.218.4574.747)
37. Tjalling Charles Koopmans, "Ordering of Wave Functions and Eigenenergies to the Individual Electrons of an Atom," *Physica* 1 (1933): 104–13. doi:[10.1016/S0031-8914\(34\)90011-2](https://doi.org/10.1016/S0031-8914(34)90011-2)
38. Robert G. Parr, László V. Szentpály, and Shubin Liu, "Electrophilicity Index," *Journal of the American Chemical Society* 121, no. 9 (1999): 1922–4. doi:[10.1021/ja983494x](https://doi.org/10.1021/ja983494x)
39. Amyand David Buckingham, "Permanent and Induced Molecular Moments and Long-Range Intermolecular Forces," *Advances in Chemical Physics* 12 (1967): 107–42. doi:[10.1080/00268979600100491](https://doi.org/10.1080/00268979600100491)
40. Alan E. Reed, Larry A. Curtiss, and Frank Weinhold, "Intermolecular Interactions from a Natural Bond Orbital, Donor-Acceptor Viewpoint," *Chemical Reviews* 88, no. 6 (1988): 899–926. doi:[10.1021/cr00088a005](https://doi.org/10.1021/cr00088a005)
41. Seiji Tsuzuki, Tadafumi Uchimar, Kazunari Matsumura, Masuhiro Mikami, and Kazutoshi Tanabe, "Torsional Potential of Biphenyl: Ab Initio Calculations with the Dunning Correlation Consisted Basis Sets," *The Journal of Chemical Physics* 110, no. 6 (1999): 2858–61. doi:[10.1063/1.477928](https://doi.org/10.1063/1.477928)
42. J. C. Sancho-García, and A. J. Pérez-Jiménez, "A Theoretical Study of the Molecular Structure and Torsional Potential of Styrene," *Journal of Physics B: Atomic, Molecular and Optical Physics* 35, no. 6 (2002): 1509–23. doi:[10.1088/0953-4075/35/6/308](https://doi.org/10.1088/0953-4075/35/6/308)
43. J. C. Sancho-García, and A. J. Pérez-Jiménez, "Nitrobenzene Rotational Energy Barrier: A Survey of Several ab Initio Methods," *The Journal of Chemical Physics* 119, no. 10 (2003): 5121–7. doi:[10.1063/1.1597632](https://doi.org/10.1063/1.1597632)
44. Alfred Karpfen, Cheol Ho Choi, and Miklos Kertesz, "Single-Bond Torsional Potentials in Conjugated Systems: A Comparison of ab Initio and Density Functional Results," *The Journal of Physical Chemistry A* 101, no. 40 (1997): 7426–33. doi:[10.1021/jp971606l](https://doi.org/10.1021/jp971606l)



45. E. Bright Wilson, Jr., "The Normal Modes and Frequencies of Vibration of the Regular Plane Hexagon Model of the Benzene Molecule," *Physical Review* 45, no. 10 (1934): 706–14. doi:10.1103/PhysRev.45.706
46. G. Varsanyi, *Assignments for Vibrational Spectra of Seven Hundred Benzene Derivatives*, Vol. 1:27 (London: Adam Hilger, 1974), 322–3.
47. K. Srishailam, B. Venkatram Reddy, and G. Ramana Rao, "Investigation of Torsional Potentials, Hindered Rotation, Molecular Structure and Vibrational Properties of Some Biphenyl Carboxaldehydes Using Spectroscopic Techniques and Density Functional Formalism," *Journal of Molecular Structure* 1196 (2019): 139–61. doi:10.1016/j.molstruc.2019.06.064
48. N. D. Patel, V. B. Kartha, and N. A. Narasimham, "Vibrational Spectra Dihalogenated Benzenes. I. In-Plane Vibrations," *Journal of Molecular Spectroscopy* 48, no. 2 (1973): 185–201. doi:10.1016/0022-2852(73)90185-9
49. P. Venkata Ramana Rao, K. Srishailam, B. Venkatram Reddy, and G. Ramana Rao, "Theoretical (DFT) and Experimental (FT-IR & FT Raman) Approach to Investigate the Molecular Geometry and Vibrational Properties of 2,5- and 2,6-Dihydroxytoluenes," *Journal of Molecular Structure* 1240 (2021): 130617. doi:10.1016/j.molstruc.2021.130617
50. P. Muralidhar Rao, and G. Ramana Rao, "Vibrational Spectra and Normal Coordinate Analysis of Monohalogenated Nitrobenzenes," *Journal of Raman Spectroscopy* 20, no. 8 (1989): 529–40. doi:10.1002/jrs.1250200809
51. K. Srishailam, K. Ramaiah, K. Laxma Reddy, B. Venkatram Reddy, and G. Ramana Rao, "DFT Simulation of Barrier Heights, Infrared and Raman Spectra, and Investigation of Vibrational Characteristics of 2-((2-Aminopyridin-3-yl) Methylene) Hydrazinecarbothioamide and Its N-Methyl Variant," *Molecular Simulation* 48, no. 15 (2022): 1315–29. doi:10.1080/08927022.2022.2086277
52. K. Ramaiah, K. Srishailam, K. Laxma Reddy, B. Venkatram Reddy, and G. Ramana Rao, "Synthesis, Crystal and Molecular Structure, and Characterization of 2-((2-Aminopyridin-3-yl)Methylene)-N-Ethylhydrazinecarbothioamide Using Spectroscopic (<sup>1</sup>H and <sup>13</sup>C NMR, FT-IR, FT-Raman, UV-Vis) and DFT Methods and Evaluation of Its Anticancer Activity," *Journal of Molecular Structure* 1184 (2019): 405–17. doi:10.1016/j.molstruc.2019.02.060
53. Hans-Otto Kalinowski, Stefan Berger, and Siegmur Braun, *Carbon-13 NMR Spectroscopy* (London: John Wiley & Sons, 1991), 792.
54. Kalevi Pihlaja, and Erich Kleinpeter, *Carbon-13 NMR Chemical Shifts in Structural and Spectrochemical Analysis* (New York: VCH Publishers, 1994).
55. P. S. Kalsi, *Spectroscopy of Organic Compounds* (New Delhi: New Age International Publishers, 2004. ).
56. Cheol Ho Choi, and Miklos Kertesz, "Conformational Information from Vibrational Spectra of Styrene, Trans-Stilbene, and Cis-Stilbene," *The Journal of Physical Chemistry A* 101, no. 20 (1997): 3823–31. doi:10.1021/jp970620v
57. I. Fleming, *Frontier Orbitals and Organic Chemical Reactions* (London: John Wiley, 1976).
58. Serap Yazıcı, Çiğdem Albayrak, Ismail Erdem Gümrükçüoğlu, Ismet Senel, and Orhan Büyükgüngör, "Experimental and Quantum Chemical Computational Study of (E)-1-[5-(3,4-Dimethylphenyldiazenyl)-2-Hydroxyphenyl]Ethanone," *Spectrochimica Acta. Part A, Molecular and Biomolecular Spectroscopy* 93 (2012): 208–13. doi:10.1016/j.saa.2012.02.092
59. Michael D. Diener, and John M. Alford, "Isolation and Properties of Small-Bandgap Fullerenes," *Nature* 393, no. 6686 (1998): 668–71. doi:10.1038/31435
60. S. H. Yang, C. L. Pettiette, J. Conceicao, O. Cheshnovsky, and R. E. Smalley, "Ups of Buckminsterfullerene and Other Large Clusters of Carbon," *Chemical Physics Letters* 139, no. 3–4 (1987): 233–8. doi:10.1016/0009-2614(87)80548-1
61. H. Handschuh, G. Ganteför, B. Kessler, P. S. Bechthold, and W. Eberhardt, "Stable Configurations of Carbon Clusters: Chains, Rings, and Fullerenes," *Physical Review Letters* 74, no. 7 (1995): 1095–8. doi:10.1103/PhysRevLett.74.1095
62. Ralph G. Pearson, "Absolute Electronegativity and Hardness Correlated with Molecular Orbital Theory," *Proceedings of the National Academy of Sciences of the United States of America* 83, no. 22 (1986): 8440–1. doi:10.1073/pnas.83.22.8440
63. Zeynep Demircioğlu, Çiğdem Albayrak Kaştaş, and Orhan Büyükgüngör, "The Spectroscopic (FT-IR, UV-Vis), Fukui Function, NLO, NBO, NPA and Tautomerism Effect Analysis of (E)-2-[(2-Hydroxy-6-Methoxybenzylidene)Amino]Benzonitrile," *Spectrochimica Acta. Part A, Molecular and Biomolecular Spectroscopy* 139 (2015): 539–48. doi:10.1016/j.saa.2014.11.078
64. G. Ramesh, and B. Venkatram Reddy, "Barrier Potential, Structure (Monomer and Dimer), Inter- and Intra-Molecular Interactions, Vibrational Analysis, Fukui Functions, MESP, NBO, UV and NMR Analysis of Pyridine-3-Carboxylic Acid Using Spectroscopic and DFT Approach," *Polycyclic Aromatic Compounds* (2022): 1–18. doi:10.1080/10406638.2022.2046614
65. S. Renuga, M. Karthikesan, and S. Muthu, "FTIR and Raman Spectra, Electronic Spectra and Normal Coordinate Analysis of N,N-Dimethyl-3-Phenyl-3-Pyridin-2-yl-Propan-1-Amine by DFT Method,"

- Spectrochimica Acta. Part A, Molecular and Biomolecular Spectroscopy* 127 (2014): 439–53. doi:10.1016/j.saa.2014.02.068
66. R. Shahidha, A. Abdulaziz Al-Saadi, and S. Muthu, “Vibrational Spectroscopic Studies, Normal Co-Ordinate Analysis, First Order Hyperpolarizability, HOMO–LUMO of Midodrine by Using Density Functional Methods,” *Spectrochimica Acta. Part A, Molecular and Biomolecular Spectroscopy* 134 (2015): 127–42. doi:10.1016/j.saa.2014.06.033
67. Yu-Xi Sun, Qing-Li Hao, Wen-Xian Wei, Zong-Xue Yu, Lu-De Lu, Xin Wang, and Yi-Shi Wang, “Experimental and Density Functional Studies on 4-(4-Cyanobenzylideneamino)Antipyrine,” *Molecular Physics* 107, no. 3 (2009): 223–35. doi:10.1080/00268970902769471
68. Ali Ben Ahmed, Habib Feki, Younes Abid, Habib Boughzala, C. Minot, and Adnen Mlayah, “Crystal Structure, Vibrational Spectra and Theoretical Studies of L-Histidinium Dihydrogen Phosphate-Phosphoric Acid,” *Journal of Molecular Structure* 920, no. 1–3 (2009): 1–7. doi:10.1016/j.molstruc.2008.09.029
69. Jose P. Abraham, D. Sajan, Venkataraya Shettigar, S. M. Dharmaparakash, I. Némec, I. Hubert Joe, and V. S. Jayakumar, “Efficient  $\pi$ -Electron Conjugated Push-Pull Nonlinear Optical Chromophore 1-(4-Methoxyphenyl)-3-(3,4-Dimethoxyphenyl)-2-Propen-1-One: A Vibrational Spectral Study,” *Journal of Molecular Structure* 917, no. 1 (2009): 27–36. doi:10.1016/j.molstruc.2008.06.031
70. Seda G. Sagdinc, and Aslı Esme, “Theoretical and Vibrational Studies of 4,5-Diphenyl-2-2 Oxazole Propionic Acid (Oxaprozoin),” *Spectrochimica Acta. Part A, Molecular and Biomolecular Spectroscopy* 75, no. 4 (2010): 1370–6. doi:10.1016/j.saa.2010.01.004
71. Chantal Andraud, Thierry Brotin, Chantal Garcia, Fabienne Pelle, Philippe Goldner, Bernard Bigot, and Andre Collet, “Theoretical and Experimental Investigations of the Nonlinear Optical Properties of Vanillin, Polyvanillin, and Bisvanillin Derivatives,” *Journal of the American Chemical Society* 116, no. 5 (1994): 2094–102. doi:10.1021/ja00084a055
72. Victor M. Geskin, Christoph Lambert, and Jean-Luc Brédas, “Origin of High Second- and Third-Order Nonlinear Optical Response in Ammonio/Borato Diphenylpolyene Zwitterions: The Remarkable Role of Polarized Aromatic Groups,” *Journal of the American Chemical Society* 125, no. 50 (2003): 15651–8. doi:10.1021/ja035862p
73. Masayoshi Nakano, Harunori Fujita, Masahiro Takahata, and Kizashi Yamaguchi, “Theoretical Study on Second Hyperpolarizabilities of Phenylacetylene Dendrimer: Toward an Understanding of Structure – Property Relation in NLO Responses of Fractal Antenna Dendrimers,” *Journal of the American Chemical Society* 124, no. 32 (2002): 9648–55. doi:10.1021/ja0115969
74. D. Sajan, H. Joe, V. S. Jayakumar, and J. Zaleski, “Structural and Electronic Contributions to Hyperpolarizability in Methyl p-Hydroxy Benzoate,” *Journal of Molecular Structure* 785, no. 1–3 (2006): 43–53. doi:10.1016/j.molstruc.2005.09.041
75. E. Artém Masunov, Arman Tannu, A. Alexander Dyakov, D. Anastasia Matveeva, Alexandra Ya Freidzon, V. Alexey Odinkov, and A. Alexander Bagaturyants, “First Principles Crystal Engineering of Nonlinear Optical Materials. I. Prototypical Case of Urea,” *The Journal of Chemical Physics* 146, no. 24 (2017): 244104. doi:10.1063/1.4986793
76. C. Cassidy, J. M. Halbout, W. Donaldson, and C. L. Tang, “Nonlinear Optical Properties of Urea,” *Optics Communications* 29, no. 2 (1979): 243–6. doi:10.1016/0030-4018(79)90027-0
77. M. Arivazhagan, and S. Jeyavijayan, “Vibrational Spectroscopic, First-Order Hyperpolarizability and HOMO, LUMO Studies of 1,2-Dichloro-4-Nitrobenzene Based on Hartree-Fock and DFT Calculations,” *Spectrochimica Acta. Part A, Molecular and Biomolecular Spectroscopy* 79, no. 2 (2011): 376–83. doi:10.1016/j.saa.2011.03.036
78. Gerhard Herzberg, *Infrared and Raman Spectra of Polyatomic Molecules, Vol. 2, Molecular Spectra and Molecular Structure*, 1st ed. (New York: D. Van Nostrand Company, 1945).
79. Kenneth S. Pitzer, *Molecular Structure and Statistical Thermodynamics, Vol. 1, World Scientific Series in 20th Century Chemistry* (Singapore: World Scientific, 1993).
80. Mohammad M. Ghahremanpour, Paul J. van Maaren, Jonas C. Ditz, Roland Lindh, and David van der Spoel, “Large-Scale Calculations of Gas Phase Thermochemistry: Enthalpy of Formation, Standard Entropy, and Heat Capacity,” *The Journal of Chemical Physics* 145, no. 11 (2016): 114305. doi:10.1063/1.4962627
81. V. Balachandran, and V. Karunakaran, “Quantum Mechanical Study of the Structure and Vibrational Spectroscopic (FT-IR and FT-Raman), First-Order Hyperpolarizability, NBO and HOMO – LUMO Studies of 4-Bromo-3-Nitroanisole,” *Spectrochimica Acta. Part A, Molecular and Biomolecular Spectroscopy* 106 (2013): 284–98. doi:10.1016/j.saa.2012.12.070
82. Leena Rajith, A. K. Jissy, Krishnapillai Girish Kumar, and Ayan Datta, “Mechanistic Study for the Facile Oxidation of Trimethoprim on a Manganese Porphyrin Incorporated Glassy Carbon Electrode,” *The Journal of Physical Chemistry C* 115, no. 44 (2011): 21858–64. doi:10.1021/jp208027s
83. J. P. Foster, and F. Weinhold, “Natural Hybrid Orbitals,” *Journal of the American Chemical Society* 102, no. 24 (1980): 7211–8. doi:10.1021/ja00544a007



84. Jana Chocholoušová, Vladimír Špirko, and Pavel Hobza, "First Local Minimum of the Formic Acid Dimer Exhibits Simultaneously Red-Shifted O-H...O and Improper Blue-Shifted C-H...O Hydrogen Bonds," *Physical Chemistry Chemical Physics* 6, no. 1 (2004): 37–41. doi:10.1039/B314148A
85. E. D. Glendenning, A. E. Reed, J. E. Carpenter, and F. Weinhold, *NBO Version 3.1* (Madison, WI: TCI, University of Wisconsin, 1998).
86. M. Suhasini, E. Sailatha, S. Gunasekaran, and G. R. Ramkuma, "Vibrational and Electronic Investigations, Thermodynamic Parameters, HOMO and LUMO Analysis on Lornoxicam by Density Functional Theory," *Journal of Molecular Structure* 1100 (2015): 116–28. doi:10.1016/j.molstruc.2015.07.003
87. M. Govindarajan, M. Karabacak, S. Periandy, and S. Xavier, "Vibrational Spectroscopic Studies, NLO, HOMO–LUMO and Electronic Structure Calculations of  $\alpha,\alpha,\alpha$ -Trichlorotoluene Using HF and DFT," *Spectrochimica Acta. Part A, Molecular and Biomolecular Spectroscopy* 94 (2012): 53–64. doi:10.1016/j.saa.2012.03.074
88. C. Muñoz-Caro, A. Niño, M. L. Senent, J. M. Leal, and S. Ibeas, "Modeling of Protonation Processes in Acetohydroxamic Acid," *The Journal of Organic Chemistry* 65, no. 2 (2000): 405–10. doi:10.1021/jo991251x
89. Eolo Scrocco, and Jacopo Tomasi, "Electronic Molecular Structure, reactivity and intermolecular Forces: An Euristic Interpretation by Means of Electrostatic Molecular Potentials," *Advances in Quantum Chemistry* 11 (1979): 115–93. doi:10.1016/S0065-3276(08)60236-1
90. F. Javier Luque, Josep Maria López, and Modesto Orozco, "Perspective on "Electrostatic Interactions of a Solute with a Continuum. A Direct Utilization of ab Initio Molecular Potentials for the Prevision of Solvent Effects,"" *Theoretical Chemistry Accounts* 103, no. 3–4 (2000): 343–5. doi:10.1007/s002149900013
91. Nora Okulik, and Alicia H. Jubert, "Theoretical Analysis of the Reactive Sites of Non-Steroidal anti-Inflammatory Drugs," *Internet Electronic Journal of Molecular Design* 4 (2005): 17–30. BioChem Press).
92. Subhash S. Pingale, Shridhar R. Gadre, and Libero J. Bartolotti, "Electrostatic Insights into the Molecular Hydration Process: A Case Study of Crown Ethers," *The Journal of Physical Chemistry A* 102, no. 49 (1998): 9987–92. doi:10.1021/jp982444b
93. K. V. Jovan Jose, and Shridhar R. Gadre, "An ab Initio Investigation on  $(\text{CO}_2)_n$  and  $\text{CO}_2(\text{Ar})_m$  Clusters: Geometries and IR Spectra," *The Journal of Chemical Physics* 128, no. 12 (2008): 124310. doi:10.1063/1.2838202
94. Neetha Mohan, Cherumuttathu H. Suresh, Anmol Kumar, and Shridhar R. Gadre, "Molecular Electrostatics for Probing Lone Pair- $\pi$  Interactions," *Physical Chemistry Chemical Physics* 15, no. 42 (2013): 18401–9. doi: 10.1039/c3cp53379d
95. Neetha Mohan, and Cherumuttathu H. Suresh, "Anion Receptors Based on Highly Fluorinated Aromatic Scaffolds," *The Journal of Physical Chemistry. A* 118, no. 24 (2014): 4315–24. doi:10.1021/jp501942z
96. C. H. Suresh, and Shridhar R. Gadre, "Clar's Aromatic Sextet Theory Revisited via Molecular Electrostatic Potential Topography," *The Journal of Organic Chemistry* 64, no. 7 (1999): 2505–12. doi:10.1021/jo990050q
97. Puthannur K. Anjalikrishna, Cherumuttathu H. Suresh, and Shridhar R. Gadre, "Electrostatic Topographical Viewpoint of  $\pi$ -Conjugation and Aromaticity of Hydrocarbons," *The Journal of Physical Chemistry. A* 123, no. 46 (2019): 10139–51. doi:10.1021/acs.jpca.9b09056